

Scotland's Rural College

Hybrid Semiconductor Photocatalyst Nanomaterials for Energy and Environmental Applications: Fundamentals, Designing, and Prospects

Mishra, Kirti; Devi, Nishu; Siwal, Samarjeet Singh; Gupta, Vijai Kumar; Thakur, Vijay Kumar

Published in:
Advanced Sustainable Systems

DOI:
[10.1002/adsu.202300095](https://doi.org/10.1002/adsu.202300095)

First published: 27/06/2023

Document Version
Publisher's PDF, also known as Version of record

[Link to publication](#)

Citation for published version (APA):

Mishra, K., Devi, N., Siwal, S. S., Gupta, V. K., & Thakur, V. K. (2023). Hybrid Semiconductor Photocatalyst Nanomaterials for Energy and Environmental Applications: Fundamentals, Designing, and Prospects. *Advanced Sustainable Systems*, [2300095]. <https://doi.org/10.1002/adsu.202300095>

General rights

Copyright and moral rights for the publications made accessible in the public portal are retained by the authors and/or other copyright owners and it is a condition of accessing publications that users recognise and abide by the legal requirements associated with these rights.

- Users may download and print one copy of any publication from the public portal for the purpose of private study or research.
- You may not further distribute the material or use it for any profit-making activity or commercial gain
- You may freely distribute the URL identifying the publication in the public portal ?

Take down policy

If you believe that this document breaches copyright please contact us providing details, and we will remove access to the work immediately and investigate your claim.

Hybrid Semiconductor Photocatalyst Nanomaterials for Energy and Environmental Applications: Fundamentals, Designing, and Prospects


Kirti Mishra, Nishu Devi, Samarjeet Singh Siwal,* Vijai Kumar Gupta, and Vijay Kumar Thakur*

The degradation of fossil fuel and worse environmental conditions leads to the emergence of hybrid semiconductor (SC) nanomaterials as photocatalysts. Hybrid SCs have interesting physical, mechanical, optical, chemical, and electronic characteristics. Due to these properties' absorption of light and transfer of charge takes place frequently and hence act as multifunctional surface. These materials should be attributed to their optical and electrical properties and act as multifunctional surfaces in energy production, fuel generation, environmental remediation, sensing, etc. When SCs combine with noble, non-noble metal, metal oxide, and some carbon-based materials, they explore wide applications in various fields. Photocatalysis is an effective and sustainable technology to reduce or fix energy concerns and environmental corrosion problems. By going through the extensive literature review, few topics are focused on designing and working mechanisms of hybrid materials. In this way, the present review article explains the properties, surface-interface engineering, design, and applications (energy and environmental) of hybrid nanomaterials, emphasizing their photocatalytic nature. Additionally, the appealing directions, scientific challenges, and the reasons behind the poor stability of Hybrid SC photocatalyst nanomaterials for energy and environmental applications are discussed. Finally, the concluding remarks and the current challenges with future prospects in this domain are highlighted.

1. Introduction

Semiconductors (SCs) are materials that have moderate conductivity. When SCs are mixed with various metal, non-metal, and carbon-based nanoparticles (NPs), they are known as hybrid SCs. Over many years these metal-hybrid SCs have been known as hybrid nanoparticles (HNPs). These HNPs have many applications in various fields like research, catalytic and photocatalytic reactions, optics, electronics, etc.^[1] Nowadays, these HNPs are proliferating. The shape, composition, and size of NPs are controlled by a recent fabrication approach, which leads to their use in many applications. The current synthetic methods also have unique properties.^[2] The metal-SC nano junction shows a unique characteristic of charge separation due to the absorption of light by SCs. The position of separated charges is based on different metal-SC interfaces, where the Fermi level of metals is present within the valence band (VB) and conduction band (CB) of SCs.^[3] Electrons get excited when the light is irradiated on SCs by creating a positive hole.

K. Mishra, S. S. Siwal
Department of Chemistry
M.M. Engineering College
Maharishi Markandeshwar (Deemed to be University)
Mullana-Ambala, Haryana 133207, India
E-mail: samarjeet6j1@mmumullana.org

 The ORCID identification number(s) for the author(s) of this article can be found under <https://doi.org/10.1002/adsu.202300095>

© 2023 The Authors. Advanced Sustainable Systems published by Wiley-VCH GmbH. This is an open access article under the terms of the Creative Commons Attribution License, which permits use, distribution and reproduction in any medium, provided the original work is properly cited.

DOI: 10.1002/adsu.202300095

N. Devi
Mechanics and Energy Laboratory
Department of Civil and Environmental Engineering
Northwestern University
2145 Sheridan Road, Evanston, IL 60208, USA
V. K. Gupta, V. K. Thakur
Biorefining and Advanced Materials Research Center
SRUC
Barony Campus, Parkgate, Dumfries DG1 3NE, UK
E-mail: vijay.thakur@sruc.ac.uk
V. K. Thakur
School of Engineering
University of Petroleum & Energy Studies (UPES)
Dehradun, Uttarakhand 248007, India
V. K. Thakur
Centre for Research & Development
Chandigarh University
Mohali, Punjab 140413, India

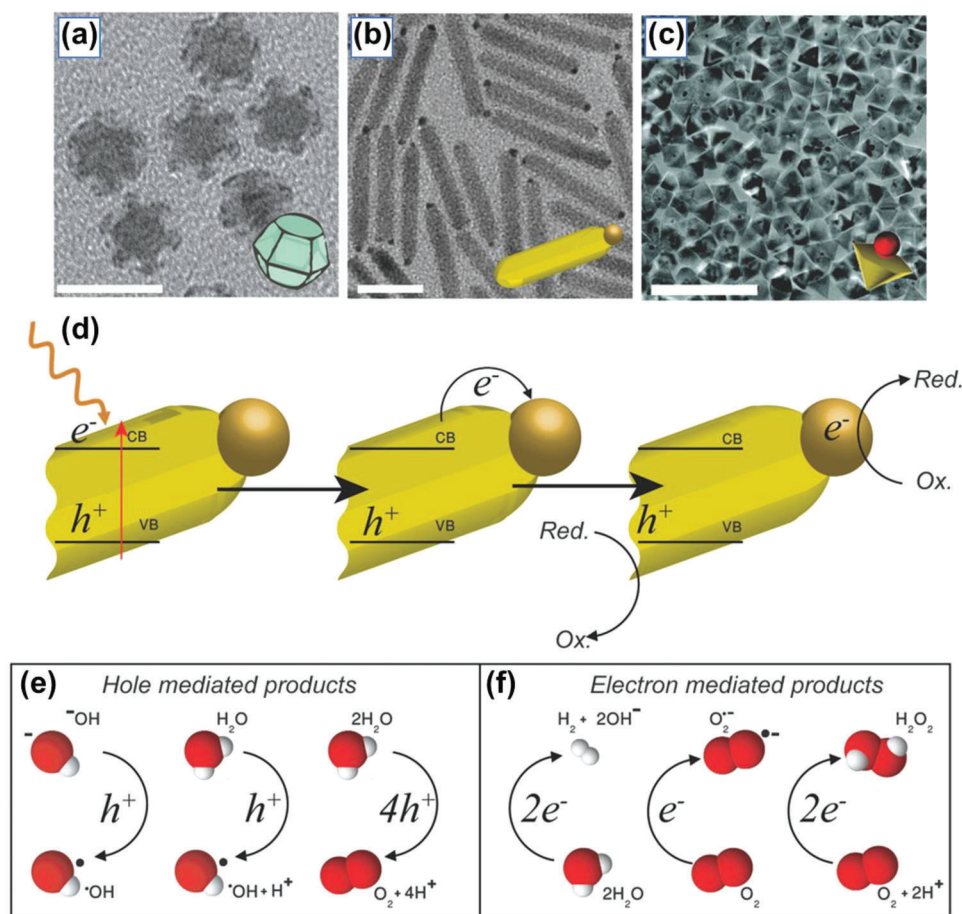


Figure 1. TEM image of a) nanocages of Cu₂S-Ru, b) NRs of CdS-Au, c) Nanopyramids of ZnO-Au, d) Schematic representation of metal-SC HNP photocatalytic mechanism with their product, e) Species oxidize by hole mediated pathway, and f) species reduced by electron mediated pathway. Reprinted with permission.^[7] Copyright 2018, Wiley-VCH GmbH.

They combine or bind with each other through coulomb interaction, known as an exciton. By recombination, the breakdown of exciton takes place; it is radiative or either by non-radiative means. Sometimes the metal in a hybrid system offers an electron sink; due to this, the excited electrons transfer to energy levels of metal from SCs. Holes remain in SCs. The property of light-induced charge transfer leads to a free charge carrier to the metallic part and is very suitable for using the energy of light for photocatalyst-based reactions, e.g., reduction of dye as investigated for nano dumbbell of CdSe-Au.^[4] HNPs also offer the customization of band alignment, and in this way, they also match the potential for a particular redox reaction to reduction potential. For many years HNPs used as a trusted photocatalyst for many photocatalyst-based applications. Further research allows the combining specific chemical and physical properties with optical properties to improve photocatalytic reactions. These HNPs are also popular in converting solar to fuel in the form of hydrogen as clean fuel via photocatalytic water splitting^[3,5] and are further used for carbon dioxide (CO₂) reduction.^[6] The Transmission electron microscopy (TEM) images of various HNPs showing in Figure 1a–c that analyzed the shape and size of NPs are shown in Figure 1a for nanocages of Cu₂S-Ru, Figure 1b for nanorods (NRs) of CdS-Au, Figure 1c for nanopyramids of

ZnO-Au. These HNPs also lead to charge separation in a redox reaction by electron transfer and hole-mediated path, as shown in Figure 1.

During photocatalytic processes, forming radicals and peroxides, or we can say that the formation of reactive oxygen species (ROS), takes place. These ROS can be used in many applications of medical and biological processes. To activate the metabolic and immune processes, the ROS act as a substrate. These processes are enzymatically activated. Further, ROS also activates some poisonous constituents that promote cell growth for photodynamic treatment.^[8] This photocatalytic nature of HNPs is also used in significant environmental cages applications like water remediation, treatment of waste based on radical-based processes, and some antibacterial performance.^[9] In addition, unique characteristics of CdS-Au HNPs come into light as 3D printing. In this process, CdS-Au acts as photo initiators.^[10] To solve the problem-related crisis of energy and environmental pollution, photocatalysis, and photo-electrocatalysis are the best suitable alternatives. But these technologies based on SCs had some problems related to the transport of photogenerated charge slow kinetics of reaction that takes place on the surface that can be solved by doing some changes in the surface by using some appropriate co-catalyst. However, it is not easy to find all the good

properties of an ideal co-catalyst using a single component material. To enhance the catalytic performance of co-catalysts HNPs are synthesized that overcome all the disadvantages of single-component materials.^[11] Fang et al.^[12] fabricated dispersed Ni NPs over a graphitic carbon matrix, i.e., Ni@C, by pyrolysis of metal–organic framework (MOF) followed by leaching of HCl that robust the photocatalytic performance of graphitic carbon nitride (g-C₃N₄) upon the exposure to visible light. This 2.0 wt.% of fabricated material Ni@C/g-C₃N₄ has a hydrogen evolution rate of 2.15 mmol h⁻¹ g⁻¹, 88 times more than pure g-C₃N₄, and performs better than Pd-gC₃N₄.^[13] The enhanced catalytic properties of the material due to the synergistic performance of both Ni NPs and graphene layers help in the separation of photo-generated electrons and also suppress the electron-hole pair recombination.

Further, it was found that hybrid SCs based on graphene oxide (GO) act as promising photocatalysts for photocatalytic applications. During the photocatalytic performance in HNPs, the electrons or photons jump into the CB and create a hole into the VB by gaining energy equal to or higher than the band energy gap. Further, these photons move over the nanocomposites' surface to proceed with photocatalytic reactions by redox reactions.^[14] In the field of photocatalysts to perform photocatalysis and electro-photocatalysis, silicon carbide (SiC) is the best option due to its good electrical properties.^[15]

In heterogeneous catalysis, single-atom catalysts are extensively used for complete metal-active sites with controlled morphology and well-distinct locations.^[16] To promote the area of photocatalysis, it is essential to develop a simple, competent, and eco-friendly way to make good photocatalysts with better activity.^[17] Herein this review article, we will discuss some hybrid SC nanomaterials as multifunctional surfaces, primarily emphasizing their energy and environmental applications. We will also discuss the photocatalytic mechanism of hybrid SCs with their designing, surface-interface engineering, and properties. Lastly, we have concluded our topic with current challenges and possible prospects in this field.

2. Properties of Hybrid Semiconductors

Hybrid SCs are formed by combining the two materials within a single particle. This combination improves materials' intrinsic properties, i.e., metal and SCs. As we know, SCs have two bands one is a lower energy VB and the other with a higher energy band CB, and the gap between these bands is known as the forbidden energy gap. The properties of these SCs depend on this energy gap. The E_g of some widely used SCs in their various states is given in **Table 1**. Some of the properties are discussed in detail in the following sections.

2.1. Optical Properties

The hybrid structure of metal and SCs leads to the formation of some new electronic states at the interface; due to this, the optical behavior of hybrid systems is different compared to metal and SCs. Hybrid SCs are excellent materials that exhibit versatile properties like conversion of solar energy into electrical energy, photocatalysis, etc. These applications of hybrid SCs are based

Table 1. Forbidden energy gap of some SCs in its different form modified from Ref. [18].

Semiconductors	Type	Band Gap in eV		
		Bulk	Nanoparticles	Hybrid form
TiO ₂	n-type	3.0	3.20	2.75 in Ag/TiO ₂
SnO ₂	n-type	3.64	3.59	3.39 in Ag/SnO ₂
ZnS	n-type	3.91 or 3.54	3.7 or 3.68	–
ZnO	n-type	3.37	3.18	2.81 in Ag/ZnO
CdS	n-type	2.42	2.62	2.42 in Ag/CdS
SnS ₂	n-type	2.2	2.24	–
α-Fe ₂ O ₃	p-type	2.2	2.2	–
SnS	p-type	1.1	1.3 to 1.39	1.25 in SnS/AuPd
Ag ₂ S	p-type	0.9	1.0	1.43 in Ag@Ag ₂ S
CuO	p-type	1.2	2.77	2.45 in Ag/CuO
Co ₃ O ₄	p-type	1.96	0.74 and 2.07	1.23 in Ag@Co ₃ O ₄

on the absorption of light. An example of CdS-Au shows absorption spectra in the near UV and visible regions. The CdS-Au absorbance increased toward high photon energy because of bound electron excitation in higher-level bands in metal and SC parts. Further, if the particle size of metal and SC is too small, then light absorption is more than scattering of light. The absorption spectrum of a hybrid SC gives information about the optical resonance. The absorption of light is also done for water splitting to produce fuels. The device used for this purpose consists of some materials that absorb light and does charge separation. For the absorption of visible light, SCs are used. Due to the low band gap, hybrid SCs are very suitable for this purpose. Several materials can absorb visible light, shown in **Figure 2**, with their band energies.^[19]

Fluorescence quenching is one of the known optical effects that occur due to metal growth. The decrease in the fluorescence intensity results in the transfer of charge from the exciting part of the SC to the metal. As a result of this mechanism, the period of fluorescence decreases with an increase in the nonradiative rate.^[20] Comparison between sample A's photoluminescence (PL) spectra is made with sample B over different temperatures (**Figure 3**). PL spectra of both samples are found to be the same at 25 °C. PL spectra move toward the lower photon energy while the temperature decreases from 300 K to 20 K. In **Figure 3a**, a featureless PL spectrum obtained within the range of 20–300 K of sample A is broad. **Figure 3b** shows sample B's two distinct PL bands at temperatures 200 K ≥ T ≥ 100 K. **Figure 3c** shows the PL spectra of both samples A and B at a temperature of 20 K that are very dissimilar: the peak of PL spectra for sample A is obtained at ≈1.03 eV having ≈100 meV full width at half maximum (FWHM), on the other hand for B sample the peak of PL spectra is obtained at ≈0.93 eV having 50 meV FWHM. In samples A and B, we constantly found 2D clusters having a chain-like combination, each characteristically comprising not more than 10 NCs (**Figure 3d**, inset). Thus, it is concluded that at a lower temperature, sample C's PL spectra are broader compared to the PL spectra of sample B (50 meV) but narrower than the PL spectra of sample A (100 meV). The PL peak was also found between samples A (1.03 eV) and sample B (0.93 eV). In response to

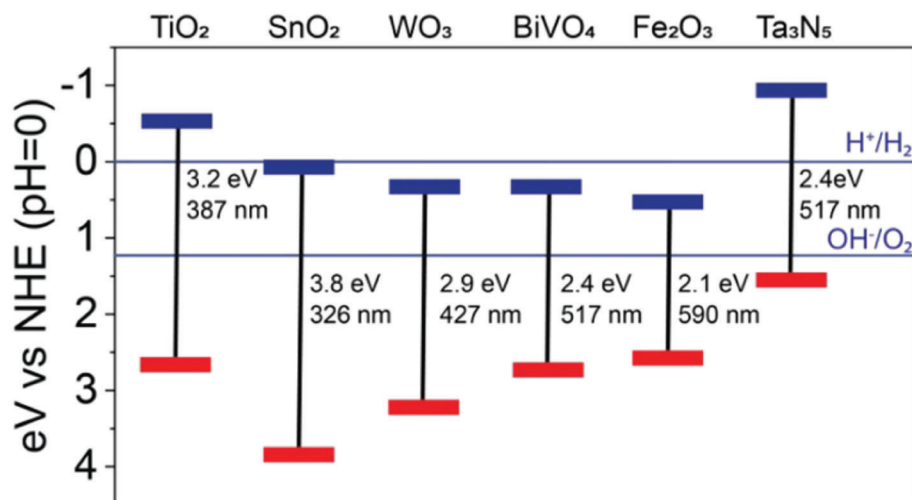


Figure 2. Various SCs conduction and valence band energies for selection in water splitting application. Reprinted with permission.^[19] Copyright 2020, American Chemical Society.

desired expectations, it was found that in sample C, the PL peak is found at 0.94 eV, and PL spectrum FWHM is ≈ 76 nm at $T = 20$ K (Figure 3d).

At 25 °C, both donor-to-acceptor and vice-versa, i.e., from acceptor-to-donor, the ET mechanism are probable (Figure 3e). Thus, there is no favored ET, and, comparable to that in the A sample, the PL spectrum at room temperature shows the PbS NC size dispersal and thermal expansion. With the decrease in temperature, due to decreased exciton–phonon interaction, the narrowing of the absorption as well as emission spectra takes place and also reduces the spectral overlap in donor–acceptor, and that makes FRET more specific towards size (Figure 3f).^[21]

The NPs of multifunctional hybrid SCs have significant applications in biotechnology and nanotechnology. This is because of its properties, like fluorescence enhancement and quenching effects. The shape and size of SC and metal NPs responsible for the optical properties of hybrid nanostructured materials. In this manner, by altering the shape and size of NPs and SCs, extraordinary properties are supposed to be developed in hybrid NPs. Taking this into mind, some researchers fabricated metal-SC nanostructure by using thiol-functionalized CdTe quantum dots (QDs)/quantum rods in combination with bovine serum albumin protein-conjugated Au NPs/NRs in water. This work revealed the exciton-plasmon interactions having NPs with diverse shapes and sizes. PL quenching was observed at 86% when NRs of Au were conjugated with CdTe QDs.^[22] Further, an inorganic SC-insulator system fabricated by using SiO₂ NPs film with CdSe NPs having excellent dispersion. In this system, SCs mainly decide the optical properties in the visible region due to a slight difference in the energy gap between the valence band and conduction band compared to insulators. In this manner, the insulators cannot change the properties of SCs. But if we take the UV visible regions, the insulators exhibit predominant properties over SCs. As explained above, the band gap in the SC and insulator hybrid system is shown in Figure 4. The PL intensity of SCs is increased by combining with insulators in a hybrid system.^[23]

In metal/SC core/shell arrangements, surface plasmon resonance modification is also studied, which changes by altering the thickness and type of SC shell. When it was performed, it was found that Au–Ag, Au–CdS, and Au–Ag₂S core/shell NRs exhibited longitudinal and transverse signals of surface plasmon resonance. When a metallic silver shell grows around the gold Ns, a blue shift is observed concerning the gold rod surface plasmon signal. A red shift is observed for CdS shell, which is further increased by increasing the thickness of the shell; as a result, the nearby shell refractive indexes show a change.^[24]

2.2. Electronic Properties

The set of parameters and representations that explain the electron's state and way of action inside the materials entirely is known as electronic properties. These properties describe the electron's state in the form of energy and momentum. Properties like dielectric phenomenon, electric conductance, etc. are studied under this.^[25] This behavior is also attributed toward the development of nano-electronic devices in the future. First, in the CdSe-Au nano-dumb bell shape, the synergetic electronic properties are observed in hybrid SCs NPs. Cryogenic scanning tunneling microscopy (STM) and scanning tunneling spectroscopy (STS) make the metal portion of a hybrid SC spatially separated from the SC. A similar gap is observed near the nano-dumb bell center as in bare CdSe NRs. But a sub-gap is kept near the nano-contact of metal and SCs. This action is responsible for creating a sub-gap interface form that frequently disappears as it moves toward the center of the rod.^[26] Similarly, the synergistic electronic consequences are also observed in the case of Cu₂S-Ru hybrid NPs, which show the presence of a metal-induced gap at the interface of a metal and SC.^[27] STM/STS studies show the enhanced electronic characteristics of hybrid Cu₂S-Ru cage morphology. Figure 5 displayed the comparison of $I-V$ curves and related $dI/dV-V$ spectrum for pure 14 nm Cu₂S seeds, mixed Cu₂S-Ru cage, and empty Ru cage. Figure 5a,b shows the spectra

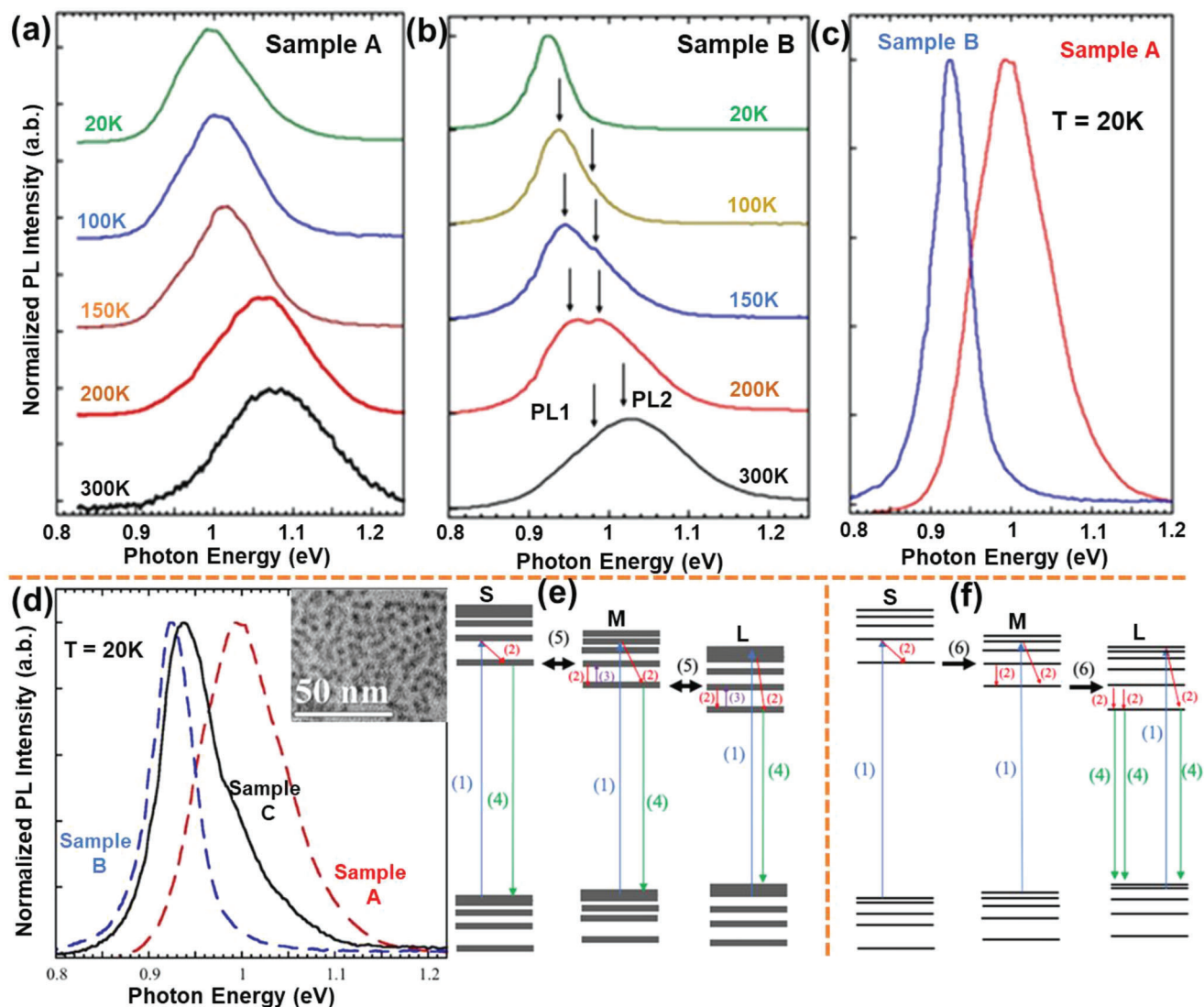


Figure 3. The PL spectrum was observed and recorded over a range of temperatures, as shown in a) sample A and b) sample B. The bands shown by arrows are PL1 and PL2 bands. c) Comparison between PL spectra of sample A and sample B takes place for the normalized low temperature. d) Normalized lower-temperature PL spectra in samples A, B, and C. The inset shows a micrograph of TEM of a sample fabricated using a solution with NC concentration $10\text{--}15\text{ mg mL}^{-1}$ (that are same in sample C) having clusters of visible PbS NCs. Representations of electronic procedures in PbS NCs situated within the FRET area having three distinct sizes within the size dispersal (labeled as S, M, and L for small, medium, and large, respectively). The procedures are shown at e) room and f) lower temperatures and comprise 1) optical absorption, 2) electron thermalization, 3) excitation by heat, 4) exciton radiative recombination, 5) energy transmission with and 6) without back transmission. Note that at a lower temperature, the narrowing of the energy levels takes place. Reprinted with permission.^[21] Copyright 2020, AIP Publishing.

of Cu_2S sources, which offer their SC nature with a band gap of approximately 1.4 eV, which is reliable with the SC gap value of Cu_2S . The blue curve in Figure 5c,d shows results measured on Ru's bare cage for tunneling spectra that represented the coulomb blockade and staircase. In some cases, periodic negative differential conductance properties are also related to staircases with green curves. Figure 5e,f prominently shows the synergetic electronic effect by STS spectra that was measured in Cu_2S -Ru. The SC gap was represented by a blue curve having a better agreement for the measurement over seeds of simple Cu_2S . This is also related to the size of STS spectra over the exposed surface of the SC. The in-gap state was shown by a green curve representing

the states of the metal-induced gap at the interface of metal and SC for the nono-dumb bell of Au-CdSe.^[2a]

2.3. Light-Induced Charge Separation

When we combine metals fragment with SCs to enhance charge transfer into a hybrid nanostructure, it leads to charge separation on the excitation of light. The transfer of excited electrons increases in SCs CB to the metal energy level. By the effect of newly developed energy band alignment at the interface of metal-SCs inside the band gap of electronic states of SCs where the

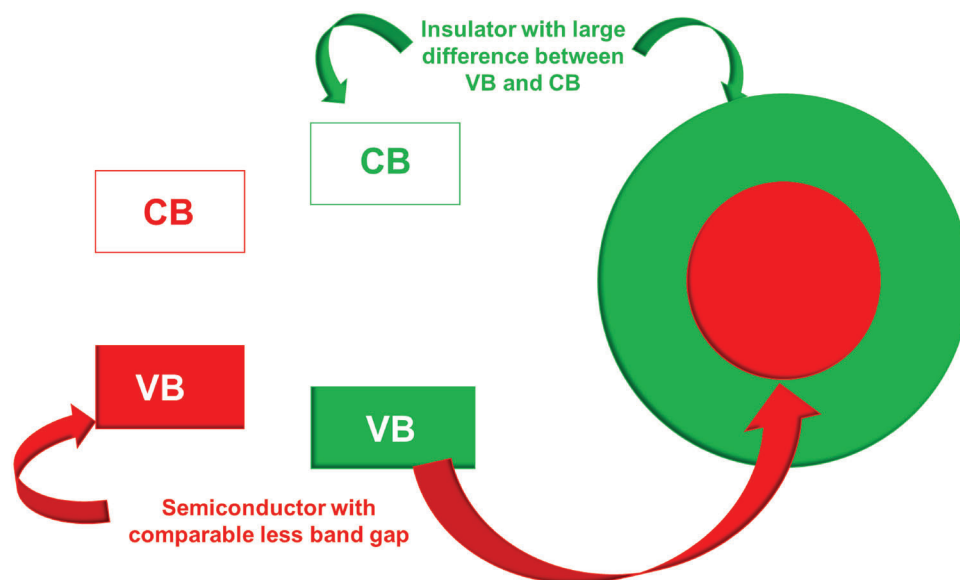


Figure 4. Representation of energy levels in SCs and insulators in the hybrid system, i.e., CB and VB on the left side; other core/shell nanostructure of the hybrid system shown on the right side of the diagram.

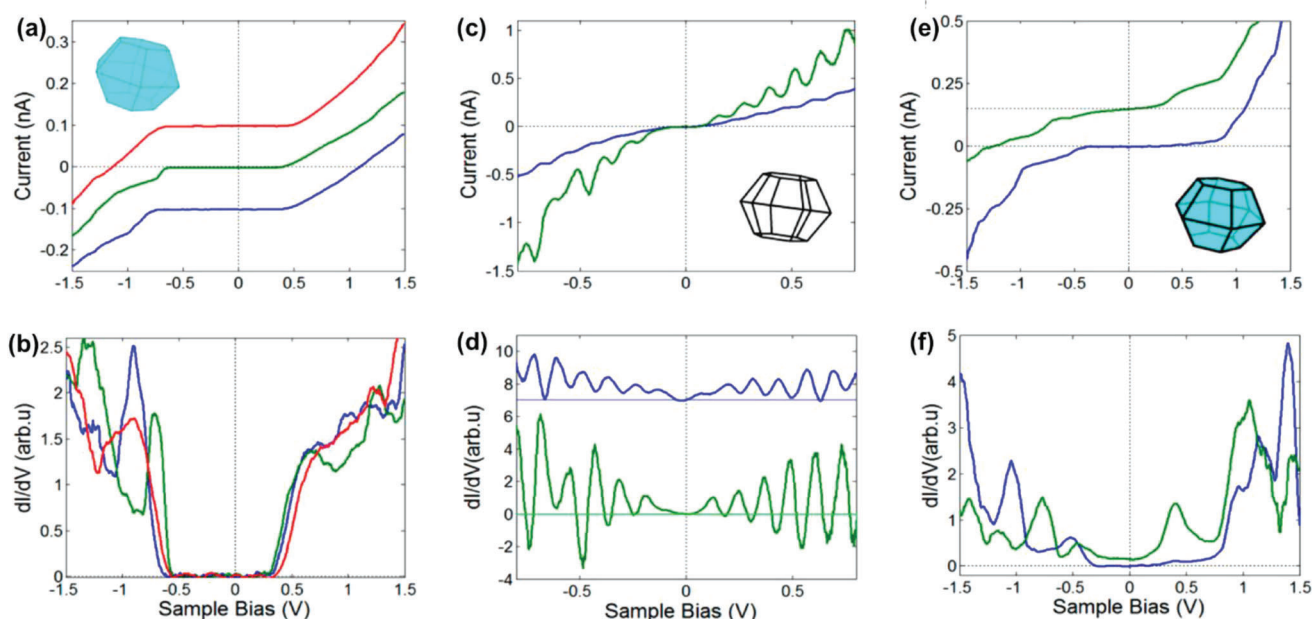


Figure 5. a,b) The basic QDs of Cu_2S displayed characteristic spectra of QDs of SC, having approximately the same value for band gap independent position of the tip, ≈ 1.4 eV in this situation. c,d) The TS measured on the bare Ru cages described the Coulomb blockade and staircase and, in some cases, negative differential conductance properties related to the stairs (with green curves). e,f) The $\text{Cu}_2\text{S}/\text{Ru}$ STS spectra show that it changes more with the surface of QDs, displaying any of the pristine SCs bandgap having in-gap states (e.g., the blue curves) or decreased gaps with an increased in-gap density of states (e.g., green curves), as well as metal-like single electron tunneling properties. Reprinted with permission.^[2a] Copyright 2014, American Chemical Society.

metal fermi level is situated. As we know, in cases of type-II & type-II shell/core arrangements, the holes present SC surface defects or some restricted boundaries. The morphology, type, and structure of these two components influence the dynamics and efficiency of the discussed process. The charge accumulation nature of various metals is different; it may be charging & capaci-

tance characteristics as shown for ZnO-Au NPs that are spherical, or as indicated for ZnO-Pt , i.e., ohmic-like contacts.^[28] The light-induced charge separation property is the most interesting because that provides the base for the photocatalytic activity of hybrid NPs.^[29] Electron hole pair generated upon excitation of absorbed photons at SC region. At the SC-metal interface,

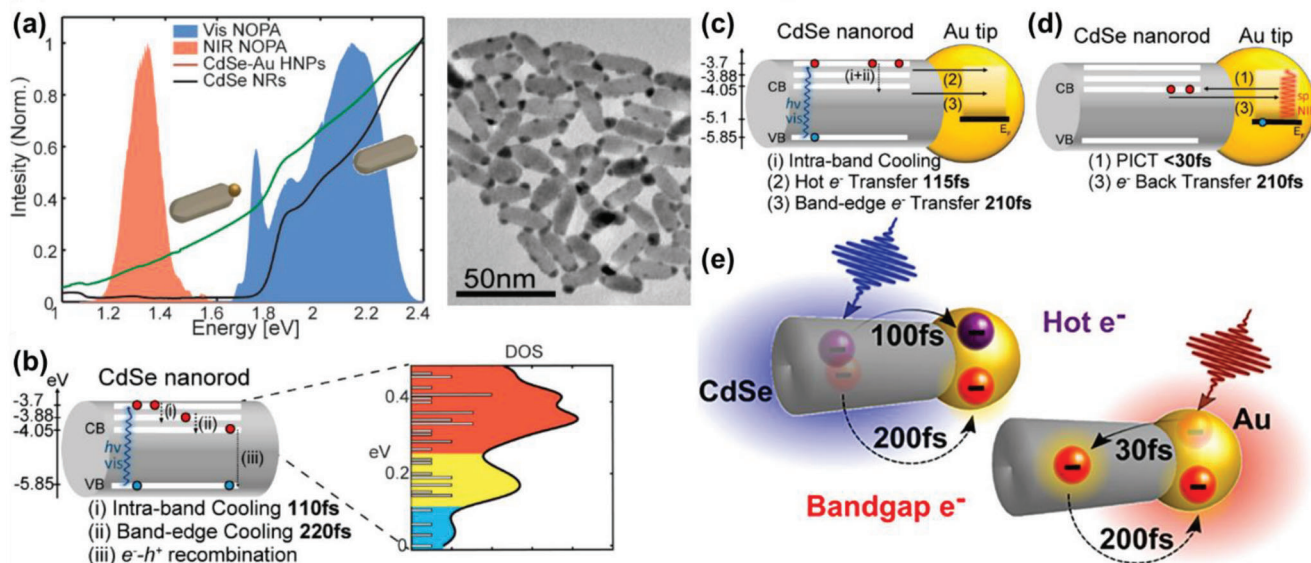


Figure 6. a) Linear absorption spectra in water for pure CdSe NRs (black curve) and CdSe-Au HNPs (green curve) normalized at 2.38 eV. The broadband pulse spectra are shown by the shaded orange and blue areas utilized in the ultrafast experiments described here. Right: TEM picture of the HNPs of CdSe-Au NRs. b) A direct report of the superfast photo-physics of bare CdSe NRs followed by photoexcitation of broadband. The calculated electron state density in CB is shown on the right side, forming three groups. The electron relaxed from the high to intermediate energy group at 110 fs and from the intermediate to lower excited state at 220 fs. c) Report of photo-physics of HNP systems of CdSe-Au NRs followed by visible broadband and d) near-infrared photoexcitation. In the previous case, the transfer of ultrafast hot electrons to Au in the 115-fs time scale participates with intraband relaxation in the CdSe and is followed by a slow (210 fs) transfer of band gap electrons to the Au. e) Schematic representation of the ultrafast transfer of hot and band electrons in CdSe-Au nano hybrid. Reprinted under the term of CC-BY license.^[33] Copyright 2021, The Authors, published by American Chemical Society.

the energy bands are aligned on both sides, which enhances the charge carrier, mainly electrons, relaxation and transfers it into the metal domain; on the other hand, holes, which are known as counter charge carriers, are only confined up to SC region. Due to this, spatial charge separation occurs, using it for photocatalytic reactions through both separate charges. Further, it was reported that sometimes the transferred charge of metal accumulates as in Au and Ag; due to this charge accumulation, the Fermi level shifted due to the charging energy of electrons. Either it is held and displayed Ohmic-like nature as in the case of Pt deposition.^[28,30] The charging of the metal segment, under radiation with a hole acceptor, will remain up to Fermi level-conduction band equilibration inside the solution.^[31] In this direction, Denis Mongin et al.^[32] investigated an ultrafast separation of charge in nano hybrid (NH) SCs by using a model arrangement of gold-tipped CdS NRs in matchstick form. To perform this experiment optical time-resolved pump-probe approach is used, exciting SCs, either metal part NPs, and probing the light-induced change to their visual behavior. Transfer of one photoexcited electron shown by outcomes from CdS to Au segment on a sub-20 fs time scale. The result indicates that such metal-SC NHs also used in photocatalysis and light harvesting applications. Further researchers investigated CdSe-Au hybrid NPs using ultrafast spectroscopy with higher temporal resolution and explained the process of electron transfer in SC and localized surface plasmon resonance (LSPR) excitations. In SCs, differentiation between hot and band gap electron transfer mechanisms occurs in the first few hundred fs. To study this, CdSe NRs are fabricated by using the surfactant-controlled growth method. The NRs have a diameter of 8.4 nm, a length of 25.1 nm, and an energy gap of

1.85 eV. After this, deposition of Au was done over the tip of CdSe NRs having size 4.1 ± 0.8 nm as shown in the TEM image of **Figure 6a** right side. The linear absorption spectra for bare CdSe NRs (black lines) and CdSe-Au HNPs (green bars) are shown in **Figure 6a**, which is normalized at 2.38 eV. The shaded orange and blue areas show the broadband pulse spectra. Further, a model of an exciton-plasmon-photocatalyst system was studied for hybrid NRs of CdSe-Au. Additionally, a combination of transient absorption spectra and 2D-electron microscopy was done to investigate this using visible light for 10 fs and near infra-red for 30 fs. The resolution for more time makes tracing and defining the route for decadent charge carrier relaxation as shown in **Figure 6(b, c)**, followed by photoexcitation of both components, i.e., plasmonic and excitonic. Further broadband photoexcitation of CdSe-Au HNPs in near infra-red is shown in **Figure 6(d)**. Ultrafast electron transfer occurs to CdSe upon excitation of LSPR, followed by electron transfer back from SC to metal that takes only 210 fs as shown in **Figure 6(e)**. This is also useful in various photocatalytic applications.^[33]

3. Hybrid Semiconductors as Photocatalysts

The most trusted energy source of human society is fossil fuels like natural gas, petroleum, coal, etc., which are present inside the earth and are very limited. The dependence of humans on fossil fuels leads to very hazardous and severe environmental and health issues. These energy sources are limited uses rapidly, so the world also faces a shortage of these potential energy sources.^[34] In addition, burning fossil fuels lead emission of CO₂ that adversely affects the environment and is responsible

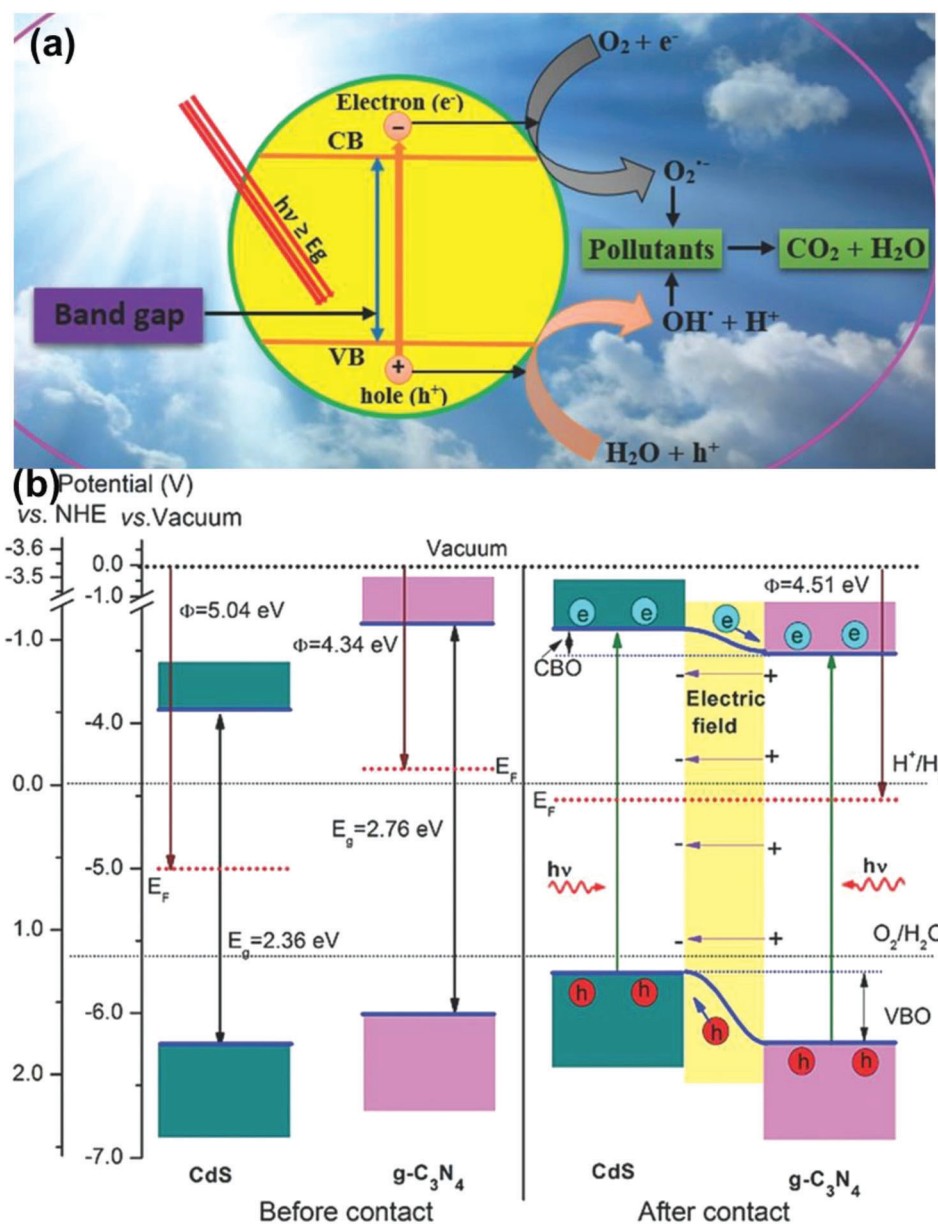
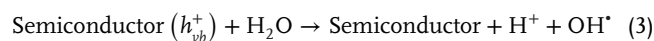
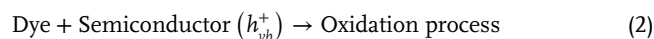


Figure 7. a) Photocatalysis process representation in SCs. b) The after and before contact edge position of a band of g-C₃N₄ and CdS. Reprinted with permission.^[36] Copyright 2017, Wiley-VCH GmbH.

for climate change. So, we need clean, clean energy sources that are low-cost, renewable, and used in place of fossil fuels.^[35] Photocatalysis and photo-electrocatalysis are the best suitable approaches from the previously known energy resources to give clean and green fuel.^[11] The basic mechanism of photocatalysis in SCs is shown in Figure 7a. Further, due to the weak interaction between CdS and g-C₃N₄, the internal electric field affected the separation of electrons and holes and restrained the recombination of e⁻/h⁺ pairs at the interface (110). The hybrid material g-C₃N₄/CdS shows high quantum efficiency on exposure to visible light compared to individual forms. Figure 7b shows the flow of electrons from g-C₃N₄ to CdS by the lower work function of g-C₃N₄. So, one can conclude that due to electrostatic induc-

tion near the interface, g-C₃N₄ shows a positive charge, and CdS shows a negative charge. In Figure 7b, CBO represents conduction band offset, VBO for valence band offset, E_g for band gap, and EF for fermi energy level.

To understand the exact mechanism of hybrid SC photocatalyst, some equations are discussed below from Equation no. (1)–(10):^[37]



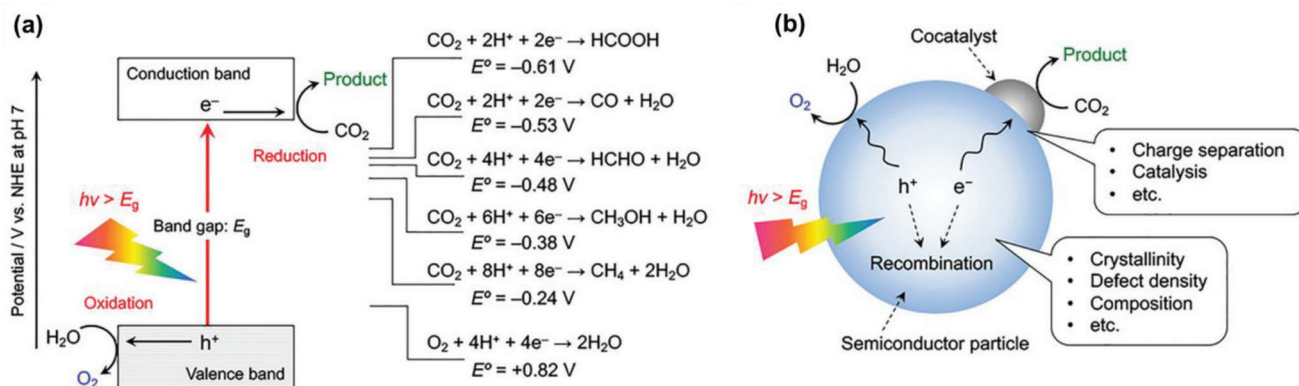
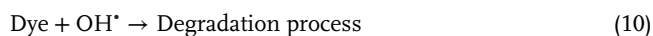
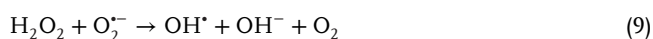
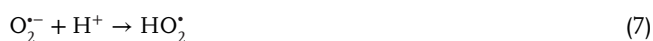
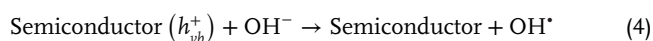


Figure 8. a) Pictorial representation of reduction of CO_2 and oxidation of H_2O with energy diagram over a SC photocatalyst. b) Representation of complete photocatalytic reaction method, with factors affecting the process. Reprinted with permission.^[38] Copyright 2019, Wiley-VCH GmbH.



The basic principle of reactions that takes place during photocatalysis when SCs are exposed to light is shown in Figure 8a. During this process, when photoexcitation of SCs takes place, CB produces electrons, and VB generates holes. When the CB minimum (CBM) and VB maximum (VBM) of the materials overlap with the redox potential of such a reaction, then only these photogenerated electrons and holes can subsequently take part in a surface redox reaction. The reactivity of photogenerated charge carriers depends on the potential of CBM and VBM and hence very significant factors in SC photocatalysis. For a photocatalytic reaction that occurs at a reasonable rate, thermodynamic and kinetic parameters must be considered while designing reactions, e.g., artificial photosynthetic responses, including H_2O and CO_2 fixation splitting. These parameters are surface catalysis and photogenerated carrier of charge (see Figure 8b). The photocatalytic activity of SCs depends on their crystalline nature; this is because such crystalline material increases the life period of photogenerated electrons and holes. To increase the charge separation ability and the chemical reaction that takes place on a SC-based photocatalyst, some co-catalyst composed of metal and metal oxide NPs must be applied over the photocatalyst surface, e.g., photocatalytic water splitting.^[38]

Further in this field, various work was done in which hybrid SCs work as a photocatalyst to produce energy. The photocatalytic reduction of CO_2 into formic acid was made using a hybrid SC-based on polymeric carbon nitride using visible light with a wavelength $>400 \text{ nm}$; when this compound is combined with a com-

plex of ruthenium show catalytic activity with a higher turnover number (TON) (>200 for 20 hours) and $>80\%$ selectivity.^[39] To improve the efficiency of charge transfer and photocatalytic performance, combining the two different SCs with dissimilar band-edge potentials was very effective. To improve the interfacial transfer of charge between semiconducting nanosheets of carbon nitride ($\text{NS-C}_3\text{N}_4$) and a supramolecular Ru(II)-Re(I) binuclear complex (RuRe), the NPs particles of rutile TiO_2 of size 5–10 nm were used as modifiers. The photocatalyst $\text{RuRe/TiO}_2/\text{NS-C}_3\text{N}_4$ hybrid can reduce CO_2 into CO under visible light with higher selectivity. It was found that CBM of rutile TiO_2 present at approximately -0.4 V vs NHE over a pH of 7, which is more positive as compared to $\text{NS-C}_3\text{N}_4$, as shown in Figure 9a. The accelerated photocatalytic behavior was explained by transient absorption spectroscopy. According to this technique, the electrons produced in $\text{TiO}_2/\text{NS-C}_3\text{N}_4$ have long lifetimes, i.e., free electrons and shallowly trapped electrons. The modifier TiO_2 acts as an excellent adsorption place for RuRe, further proved by experimental data. Due to this, the unwanted desorption of the complex decreases and results in higher catalytic performance. These changes produced by RuRe generated a new absorption band for visible light centered at 470 nm (Figure 9b); this is because of metal-to-ligand charge transfer (MLCT) excitation of RuRe, which act as the photosensitizer. Doing changes with TiO_2 , the higher adsorption of RuRe enhanced by a factor of 2.5, as shown in Figure 9c compared to bare $\text{NS-C}_3\text{N}_4$. In spite, the surface area of the modified and unmodified complex was nearly the same.^[40]

Juan Aliaga et al.^[41] observed the photocatalytic performance of the organic-inorganic laminar ZnO (stearic acid) (SA) having a band gap or energy gap (E_g) of 3.28 eV in combination with organic-inorganic hybrid V_2O_5 (hexadecyl amine)(HDA) having ($E_g = 3.28$) for the breakdown of aqueous methylene blue (MB) solution in the presence of visible light. We knew a different number of combinations, i.e., V_2O_5 and V_2O_5 -xerogel, that helped to explore the photocatalytic performances. The hybrid form of organic-inorganic hybrid SCs 2D/2D generates predictable combinations that improve the easy breakdown of selected dye, which acts as the organic contaminant model. The photocatalytic characteristics of the as-fabricated materials were tested under the same situations, and after attaining the adsorption/desorption

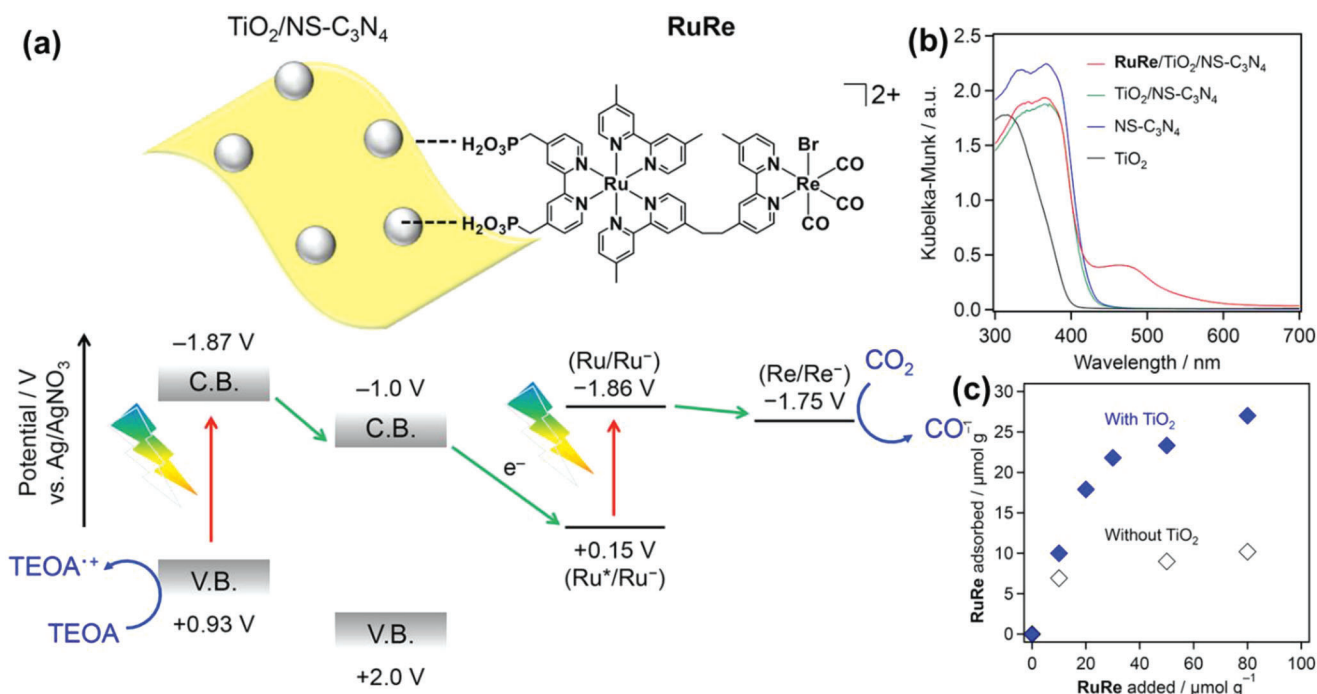


Figure 9. a) The hybrid catalyst RuRe/TiO₂/NS-C₃N₄ band position is shown with respective band energy, b) UV-visible diffuse reflectance spectra of TiO₂, NS-C₃N₄, and 8 wt% TiO₂/NS-C₃N₄. Data for 8 wt% TiO₂/NS-C₃N₄ modified with 27.0 μmol g⁻¹ RuRe is also shown. c) Adsorption isotherms of RuRe on NS-C₃N₄ at room temperature before and after modification with TiO₂ (27 wt %). Reprinted with permission.^[40] Copyright 2017, American Chemical Society.

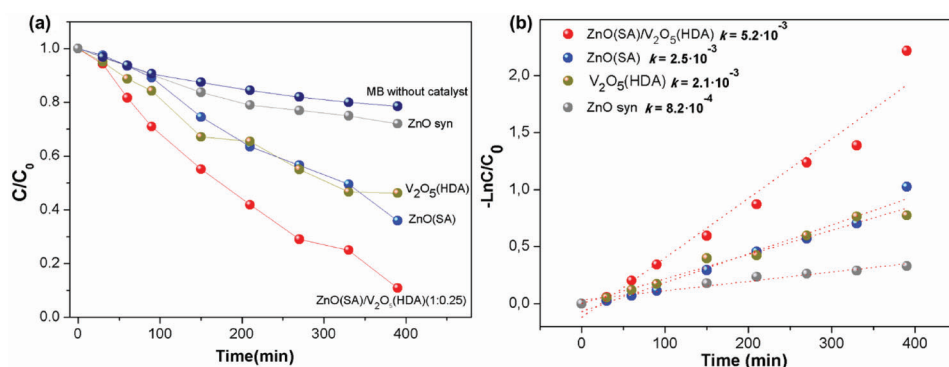


Figure 10. a) Photocatalytic activity of the samples ZnO(SA)/V₂O₅(HDA) for the decomposition of MB solution and the breakdown of MB in the absence of photocatalyst. b) Kinetics of photodegradation of MB solution that followed pseudo first-order kinetics. Reprinted under the term of CC-BY license.^[41] Copyright 2018, The Authors, published by MDPI.

equilibrium, all curves were normalized. The results indicate that the excellent photocatalytic efficiency was shown by heterojunction ZnO(SA)/V₂O₅(HDA) 1:0.25, as shown in **Figure 10a** under irradiation of visible light as we that processes related to photocatalysis are much complex in nature. Some characteristics of the kinetics of the reaction are studied in detail. The pseudo-first-order kinetics was followed by the photocatalytic degradation of methylene blue (MB), as shown in **Figure 10b**. The equation for this is $kt = \ln[C_0/C]$, where C_0 is the initial and C is the final concentration, k is the related kinetic constant, and t is the irradiation time.

The HNPs show various advantages in the field of photocatalysis-based applications. It is also suitable to apply them for light-based thermal catalysis. Kim et al. investigated the increased catalytic performance of HNPs when exposed to light, resulting in the production of hot carriers in the metal. During the investigation, they found that nanodumbbells of Pt-CdSe-Pt display an advanced turnover frequency by a factor of 2 on the exposure of light having energy more than the CdSe bandgap; on the other hand, bare Pt NPs turnover percentage does not base on irradiation of light. It was also reported that Pt NPs deposited on a GaN surface during light irradiation show variation in

their catalytic behavior toward the oxidation of CO based on the type of GaN doping. The catalytic performance of Pt NPs also depends on the hot electrons injected in Pt NPs by light irradiation. This behavior also affects the catalytic performance toward oxidation of CO, leading to a new application of these HNPs, i.e., actuators.^[42]

Further, it was found that photocatalyst based on SCs has a narrow range of absorption for sunlight and lower utilization efficiency for light. It is due to the limitations in the SCs band gap. To overcome this problem, pure metal-based plasmonic photocatalysts are used. In this case, a resonance between photons and free electrons occurs over the surface of the metal during the complete light area. Rapid fabrication of photochemical characteristics and micro-environments for the reaction will expose future-generation new multi-functional photocatalysts, which are plasmonic photocatalysts, one of which accelerates the activity of solar H₂ fuel production from pure MeOH.

Considering this concept, a multicomponent-based plasmonic NH is fabricated by using Cu NPs with tungsten carbide and tungsten (WC/W) NPs that are used as a catalyst for the production of H₂ from MeOH. This activity is supposed to increase due to the synergistic effect of plasmonic photocatalysis and reaction microenvironment. The process involves 1) Strain effect formation from W core to WC shell in WC/W core-shell composites. 2) The localized surface plasmon resonance leads by plasmonic WC/W that induce an electronic effect over the surface of WC. 3) Use of the solar spectrum is also enhanced due to the absorption of plasmonic NPs of Cu. Only 2% loading of Cu-WC/W NPs leads to the enhanced photo forming of liquid MeOH. This catalyst is highly stable and also does not produce CO_x.^[43] A plasmonic composite based on non-noble metal, i.e., Cu₆Sn₅ bimetal NPs with reduced GO (Cu₆Sn₅-rGO) absorbs a broad spectrum and shows excellent activity toward photocatalytic water splitting. The plasmonic Cu₆Sn₅ bimetal competently produces electro-hole pairs further inserted into the rGO. Both Cu₆Sn₅ and rGO give photocatalytic sites that are saturated by charge, initiating the overall water splitting and acting as plasmonic photocatalysts.^[44] Bimetallic and multimetallic NPs exhibit greater activity toward photocatalysis due to the transfer of electrons between metals. Several bimetallic NPs with elevated charge separation ability have been developed, including Au-Pd, Au-Cu, Au-Pt, etc.

Further, researchers investigated that the combination of catalytic and plasmonic metals is needed to obtain both excellent catalytic performance and good utilization of light. A hetero superstructure of Au NRs@Pd was synthesized in which nanoarray of Pd grew over the surface of AuNRs using a seed-mediated method that enhances photocatalytic activity by C-C coupling reaction.^[45] Other materials like covalent organic frameworks are also used to enhance photocatalytic performance because of their high crystallinity and good electronic and optical characteristics.^[46] Photocatalysts based on organic materials are also used due to their appropriate reductio-oxidation band positions, higher chemical stability, and more economic and suitable electronic structure. An organic photocatalyst that shows a strong response to visible light PDI-Ala (*N, N'*-bis(propionic acid)-perylene-3, 4, 9, 10-tetracarboxylic diimide) is known to have a low position of valence band with the solid ability for oxidation.^[47]

4. Surface and Interfaces Engineering of Photocatalysis

To measure the photocatalytic behavior of HNPs the surface and interface engineering are the two most important factors. A simple photocatalytic reaction kinetics proceeds in three steps:

- 1) Production of charge upon irradiation of light,
- 2) Transfer of charge over the surface of the catalyst,
- 3) Use of these charges for redox reactions.

During redox reactions, a photocatalyst transforms solar energy into chemical energy.^[48] Further improvement in the above discussed each step, enhancing the efficiency of photocatalyst, is known as engineering. By following these steps, it can develop a highly efficient catalyst. Surface engineering is a valuable method to boost the surface adsorption and activation capabilities for reaction entities; electrons or holes present in the photocatalyst or substrate surface can participate more efficiently in redox reactions. Interface engineering mainly prevents the unfavorable electron-hole combination, so it helps in coming more and more electrons and holes to reach the surface for reduction-oxidation reaction. The surface factors include facets, compositions, phases, areas, vacancies, pores, surface state, and band bending, which are significantly responsible for the catalytic performance and selectivity with the valuable purpose that these factors have an impact on the surface adsorption and activation capabilities for particular reactants.^[49] The interface is the position between two components where the charge transfer occurs. These electron holes are passed via the interface during the transfer of charge. The interface factors with interfacial compositions, defects, areas, facets, electronic coupling, and band bending strongly affect the transfer of charge and separation effectiveness.^[50] The various steps involved during surface and interface engineering of HNPs as photocatalysts are shown in **Figure 11a**. after incorporating the charge kinetics model, we need to select a more effective architectural structure. There is various type of basic architectural models in the photocatalysis process. Some of them are homogeneous for single-nanoparticle SCs, heterogeneous networks for encapsulated structures, and some interconnected structures for multi-nanoparticles in SCs, as shown in **Figure 11b**.^[51]

Different materials have various morphology known as polymorphs or multiple phases. These phases arise due to variations in the electronic structure responsible for each phase's diverse activity. Working with the engineering phase comprises taking benefit of distinctive characteristics for the required processes. Further, researchers investigated the photocatalytic evolution of H₂ in the presence of visible light enhanced 35 times with the use of 1T-MoS₂/CdS hybrid Nano nods system compared to CdS NRs.^[52]

Using the SEM, the morphology of the samples is analyzed (**Figure 12**). **Figure 12a–d** displays the morphology of 1T-MoS₂ and SV-1T-MoS₂ that looks like flowers. The variations in morphology similar to the flower are due to sulfur vacancies. **Figure 12e,f** shows the rod-shaped morphology of CdS. **Figure 12g** shows the predictable positions of VB and CB in the three photocatalysts. **Figure 12h** displays the photocatalytic production rate of NH₄⁺ of SV-1T-MoS₂ by comparing it with NRs

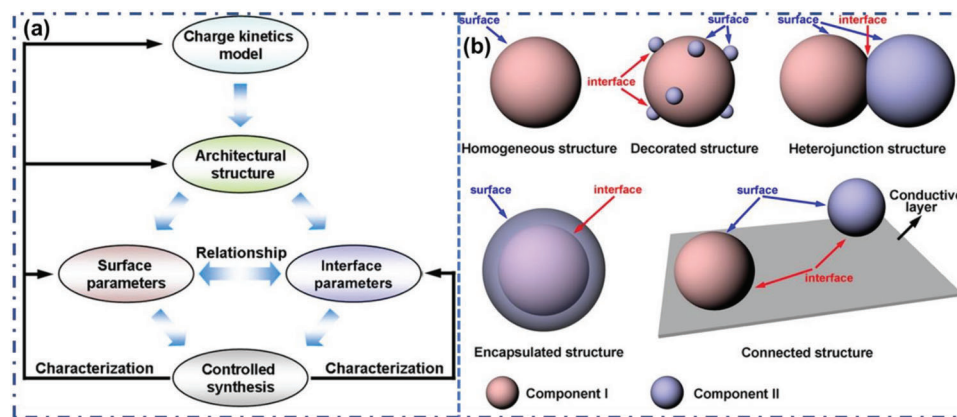


Figure 11. a) Pictorial representation of surface and interface engineering implanted during research for photocatalysis. b) The various type of interfaces and surfaces in elementary photocatalytic architectural morphology. Reprinted with permission.^[51] Copyright 2015, Wiley-VCH GmbH.

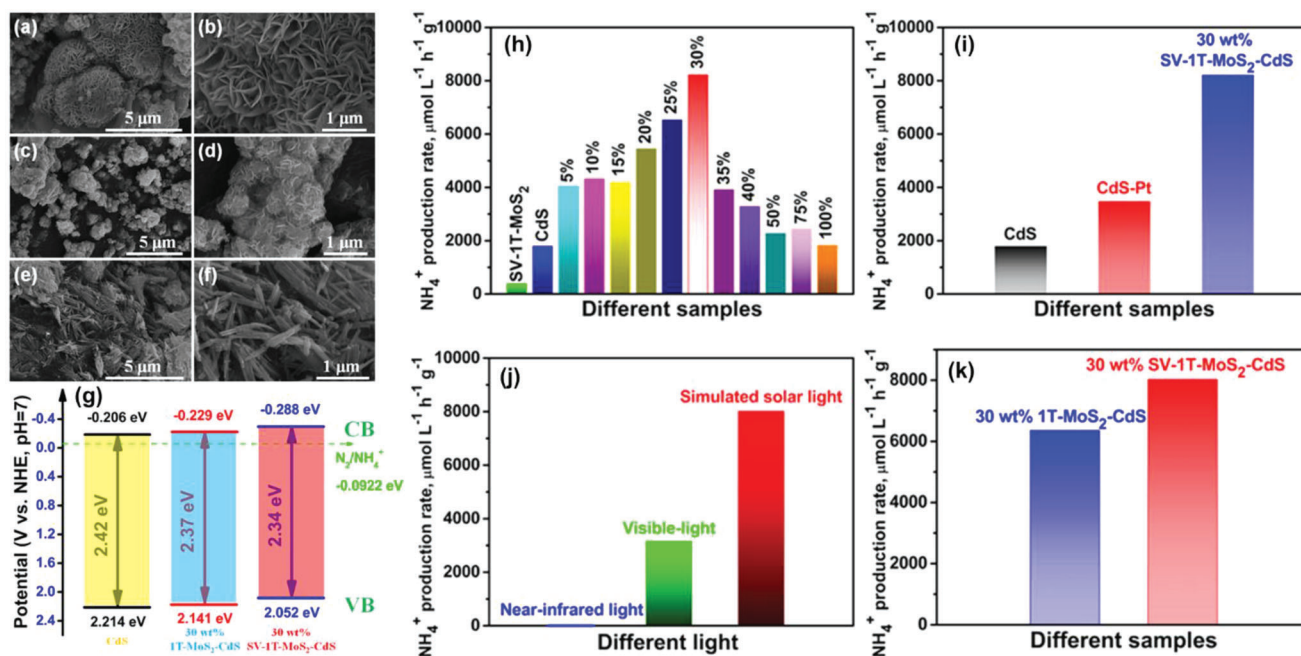


Figure 12. SEM pictures of SV-1T-MoS₂ (a,b), 1T-MoS₂ (c,d), and NRs of CdS (e,f). g) Band morphology of CdS NRs, SV-1T-MoS₂/CdS composites (30 wt.%), and 1T-MoS₂/CdS (30 wt.%). Photocatalytic production rate of NH₄⁺ on exposure to sunlight (h) for SV-1T-MoS₂, NRs of CdS, and SV-1T-MoS₂/CdS composites comprising of various quantities of cocatalysts (5, 10, 15, 20, 25, 30, 35, 40, 50, 75, and 100 wt.%) (i) by NRs of CdS, 0.1 wt.% of CdS-Pt, and SV-1T-MoS₂/CdS composites (30 wt.%). j) by SV-1T-MoS₂/CdS (30 wt.%) composites on irradiation with different light, and k) of SV-1T-MoS₂/CdS (30 wt.%) and 1T-MoS₂/CdS (30 wt.%) composites on exposure to sunlight. Reprinted with permission.^[52a] Copyright 2020, American Chemical Society.

of CdS and SV-1T-MoS₂/CdS composites with changed quantities of co-catalysts. To investigate the activity towards nitrogen fixation CdS-Pt (0.1 wt.%) was also fabricated (Figure 12i). In addition to this, the photocatalytic production rate of NH₄⁺ by SV-1T-MoS₂/CdS (30 wt.%) was also measured. For this purpose, the illuminations of different lights were done; Figure 12j represents the NH₄⁺ photocatalytic production rate of 8220.83 μmol L⁻¹ h⁻¹ g⁻¹ on exposure to solar light, which is much higher than illumination to visible light 3168.20 μmol L⁻¹ h⁻¹ g⁻¹. Further, to know the effect of defects created by sulfur and supplementary 1T phase amount in the SV-1T-MoS₂. Figure 12k shows the com-

parison between SV-1T-MoS₂/CdS (30 wt.%) and 1T-MoS₂/CdS composites (30 wt.%) for the photocatalytic production rate of NH₄⁺.

This type of improvement is also observed in the case of nanosheets of 1T-MoS₂. The functional properties of nanostructures based on noble metal are also improved by modifying the shape, size, composition, and phase of crystals. It was found that a 4H-phase Ag material also shows 100-fold high in-plane resistivity and enhanced absorption of visible light in comparison to Ag films having a face-centered cubic phase. The activity toward reaction, efficiency toward degradation of pollutants, and

material performance are also affected by surface-interface engineering. SnO_2 and PbO_2 have low oxygen evolution rates; hence they act as efficient catalysts and substrates for pollution oxidation. In this process, the rate of oxygen evolution is suppressed. To obtain the various phases of metal oxides, anodic and cathodic deposition process is also used.^[53]

5. Designing of Hybrid Semiconductor Photocatalyst Nanomaterials

The fabrication of hybrid nanoparticles is increasing day by day. Selecting the site or position where metal is deposited to prepare hybridSCs is the first step. This selection is based on the morphology of metal crystals. The structure may be seeded rods such as CdS, and CdSe/CdS seeded rods. The sites in SCs with crystal defects are also suitable for metal deposition due to the presence of a high-energy surface site. On the other hand, control of metal morphology is also essential while fabricating or designing hybrid NPs. The shape and size of metal effectively influence the surface faces and hence the photocatalytic behavior of HNPs. By considering this as we know that triangular shape Ag NPs scatter red light by developing two different quadrupole plasmon resonances, while spherical-shaped NPs scatter blue light with only one plasmon.^[2a,3] Some dual metal-based hybrid NPs are also prepared by depositing two metals over the surface of SCs by core/shell structure or by interfacial alloys. By doping this dual system, the properties of the hybrid system are greatly improved. For example, when we combine Pt/Ni and Pt/Ru/Ni alloy NPs it shows better performance toward electrooxidation of methanol than Pt NPs.^[54] Hybrid SCs work as photocatalysts, converting absorbed solar energy into electricity or electrical energy through redox reactions. For many years sulfides, metal oxides, selenides, etc., act as photocatalysts. Currently, n-type SCs (TiO_2 , Fe_2O_3 , WO_3) are widely used as photocatalysts. While designing the hybrid SC photocatalysts, some points are kept in mind to enhance the photocatalytic performance of the hybrid photocatalyst with superior performance. These points are:

- 1) Doping of SCs with metal and non-metal.
- 2) Facet engineering done by suitable methods.
- 3) Surface modification of SCs is done by combining various carbon-base materials like GO, $g\text{-C}_3\text{N}_4$, rGO, some polymeric base materials etc.
- 4) The addition of oxidants is also done in SCs to enhance photocatalytic performance.
- 5) Morphology control of particles is also a strategy to enhance the activity of photocatalysts.^[37]

Some of the methods for designing hybrid SCs by considering the above things are discussed in the following sections.

5.1. Doping of Metals and Non-Metals

As previously discussed, the various properties of SCs as photocatalyst depends on defect and impurities. The doping process introduces these defects and impurities. By doping, n- and p-type of the system obtained that act as photocatalysts of visible light.

The doping of metals can be grouped into three parts, i.e., noble metal doping, alkali metal doping, and transition metal doping. Doping lowers the energy gap between bands and hence results in the absorption of visible optical.^[55] Over the absolute energy scale, when the energy gap is high between VBM and CBM, then n- and p-type doping is challenging, as shown in various studies. n-type SCs are only formed when doped impurities can provide extra electrons to host atoms. P-type SC formed when host atom gains extra valence hole from contaminants. To adjust the band arrangement and enhance the photo response of SCs for visible light, it is more reliable to doped SCs with transition metals,^[56] metalloids,^[57] lanthanides,^[58] noble metals,^[59] alkaline earth metals,^[60] nonmetals,^[61] and rare earth metals.^[62] Due to doping, some point defect is created in SCs. When metal ions are incorporated into the SCs, it establishes an intraband state close to the VBM or CBM edge. This intraband introduction of visible light makes it easy and leads to its optical absorption. The redox energy levels are very close in many metals' ion, which leads to the optical absorption of visible light in a band gap state. The maximum absorption of visible light leads to the migration of the charge transfer between doped metal d-orbital to VB(CB) SCs. By using its surface plasma resonance effect, the noble metal doped SCs show advancement in the transfer of photo-generated charge carriers, i.e., electrons and holes, as well as improve their visible light photoelectron conversion proficiency.^[63] Ru,^[64] Rh,^[65] Pd,^[66] Pt,^[67] Au,^[68] and Ag^[69] also act as effective co-catalyst for the degradation of the organic contaminant and photocatalytic water splitting.

Out of the above-discussed co-catalyst, due to its lower overpotential and higher work function toward environmental radiation progression, Pt acts as the most competent co-catalyst. In addition to this, some lower-priced metals like Co,^[70] Ni,^[71] and Cu^[72] also act as effective co-catalyst. By doping metals, impurities levels are incorporated in the forbidden gap. Metal doping occurs according to the oxidation state and ionic radius of the host and doping atoms. The impurity level is a type of energy band unoccupied by electrons. The introduced impurity level acts as an electron donor or electron acceptor because it permits SCs to absorb visible light. Through this process, various photo responses by dopant cations were observed due to visible light.^[73]

By their unique optical and catalytic nature ZnS and CdS act as superior SCs. But their practical applications are minimal due to their lower photon efficiency and higher photo-corrosive nature. To enhance the properties of SCs it is necessary to make them heterojunction in nature, which is done by doping with transition metal ions. By using a simple chemical precipitation approach, Ni-doped ZnS-CdS hybrid material was fabricated. To know the morphology of the surface and structure of Ni/ZnS-CdS hybrid TEM analysis was done. The results of TEM are shown in **Figure 13a,b** with different magnifications and show that particles are spherical in nature. Photoluminescence (PL) studies were done at room temperature to analyse the fabricated composite's surface defect. PL om composite, i.e., Ni/ZnS-CdS shown in **Figure 13c** under 315 nm excitations. Three emission peaks, i.e., at 378, 527, and 660 nm, were observed in the PL spectrum. The result shows that Ni/ZnS-CdS hybrid composite is very useful for optical devices that emit green light.^[74]

Furthermore, Pt-doped TiO_2 displayed superior photocatalytic degradation toward nitrobenzene compared to a pure cluster of

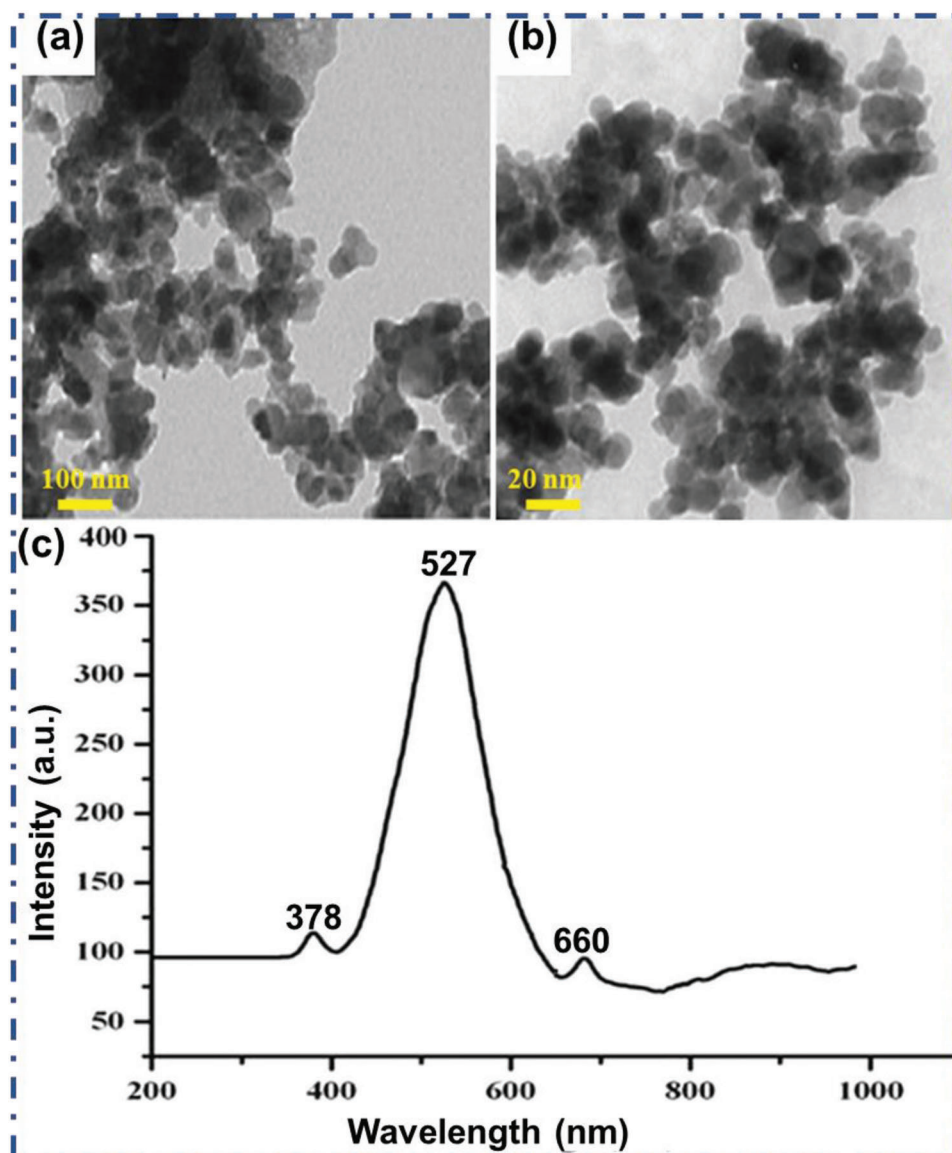


Figure 13. a,b) TEM images of hybrid composite Ni/ZnS-CdS in different magnifications showing the spherical shape of particles, c) PL spectrum of Ni/ZnS-CdS showing three peaks at 378 nm, 527 nm, and 660 nm result in green light emitting nature. Reprinted with permission.^[74] Copyright 2021, Elsevier.

Pt. The absorption of visible light ($\lambda = 400\text{--}1000\text{ nm}$) was improved by doping TiO_2 with Cu, in which Cu and Ti are 3d near the VBM. This result was obtained by studying its optical and electronic nature.^[75] Due to doping with a transition metal, the visible light photo responses of SCs increase but on the other hand, their efficiency and thermal stability decrease.^[76] Nonmetal doping is also an excellent option to enhance the visible light absorption of SCs. Nonmetal doping has been mainly acknowledged to sensitize SCs on the way to the visible light region as opposed to surface positions known to entrap photogenerated e^-/h^+ couples by metal dopants. Nonmetals can reduce the band gap by acting as a part of VB either an electronic states created by nonmetals near the VB of SCs.^[77] TiO_2 is an excellent photocatalyst with a low price, higher durability and lesser toxicity. But TiO_2 shows their activity only under UV light. The catalytic reaction

and applications of TiO_2 in visible light are hindered. By doping with non-metal or co-doping, the catalytic performance of TiO_2 can be enhanced in visible light due to a decrease in the energy band gap. Due to these excellent changes, TiO_2 can do photocatalytic degradation of organic pollutants in the presence of both UV and visible light and is used for wastewater treatment.^[78]

Nitrogen-doped TiO_2 , i.e., N- TiO_2 nanostructured, was fabricated by Park et al.^[79] using a graft polymerization process. Under irradiation with visible light, this material is used to breakdown down methylene orange dye photo catalytically due to doping with nitrogen the electronic band levels of TiO_2 reformed. Further S- TiO_2 material was fabricated by Boningari et al.^[80] via a new single-step flame spray pyrolysis process. Doping with S in TiO_2 stimulated anatase to rutile changes in the fabricated catalyst and reduced the energy of its bandgap by replacement

with cation (with S4p and S6p). These cations worked as electron trapping entities, robust the TiO₂ electrical conductivity, and upgraded the transfer of electron and hole pairs.

As a result, s-doped TiO₂ acts as a superior photocatalyst compared to bare TiO₂ in visible light. It was also known that C-TiO₂ also displayed higher photocatalytic performance. CPS/TiO₂ composites were fabricated in situ using C-TiO₂ single crystal NRs as starting materials. The doped C formed an impurity level at the oxygen site of TiO₂ in between the CB and VB of the SC. Due to this transfer of electrons takes place by this impurity band quickly; as a result, the bandgap of TiO₂ is reduced, i.e., <3.2 eV.^[81]

5.2. Co-Doping with Metals and Non-Metals

Due to the synergistic effect between two different dopants, the Co-doped NPs displayed more visible light absorption than single-doped TiO₂, and the charge carriers' lifetime also increased. The co-doping done by either nonmetal-metal,^[82] nonmetal-metalloid,^[83] nonmetal-nonmetal,^[84] or metal-metal^[85] pairs results in superior approaches to modify the band structure of SC-based photocatalyst materials having improved photo responses. It has come to know that nonmetal-metal co-doping TiO₂ can change the catalyst band edges by uplifting the VB edge and constructing the CB edge increased 0.24 eV. So, by co-doping, the bandgap decreased by approximately 2.72 eV. N and Ta are predicted to be the mark donor-acceptor pair having a band gap of 2.71 eV, which red-shifts the TiO₂ absorption edge to 457.6 nm in the visible range. This band engineering principle is also suitable to robust the photocatalytic performance of other SCs with large bandgap.^[86]

Wang et al.^[87] fabricated co-doped C, N, S-TiO₂, having different phases by applying a hydrothermal process. Compared to anatase C, N, S-TiO₂ NRs, rutile C, N, S-TiO₂ NRs displayed increased degradation competence when exposed to light having high wavelengths, although anatase C, N, S-TiO₂ NRs having a larger surface area. This shows that surface area is not essential for the superior performance of rutile-phase NRs. The robustness in photocatalytic performance is not only based on the lower energy bandgap created by the co-doping of C, N, and S in the TiO₂ lattice but also influenced by the rutile morphology of one-dimensional NRs, which encourages the active segregation of photo-generated electron and hole pairs. The NaTaO₃ also exhibited improved photocatalytic activity obtained by co-doping with Mo-N, having elevated mobility of charge carrier electrons and holes. This is due to the variety of band structures created by the Mo and N co-dopant.^[88]

Furthermore, the band situation of the Mo-N co-doped NaTaO₃ was properly present to fulfilled the thermodynamic durability of photo-oxidation and photo-reduction of H₂O. Compared to Si and F-doped TiO₂, the Si-F co-doped TiO₂ was thermodynamically more stable within generalized gradient approximation and Perdew–Burke–Ernzerhof scheme.^[89] The increased optical absorption of Si-F co-doped TiO₂ was due to the decrease in the electron transition energy from the VBM to CBM. The accelerating consequence of the photoactivity of SrTiO₃ co-doped with N and Sb was reported to increase the visible light activity because of the charge compensation. Further, the band's position in N-Sb

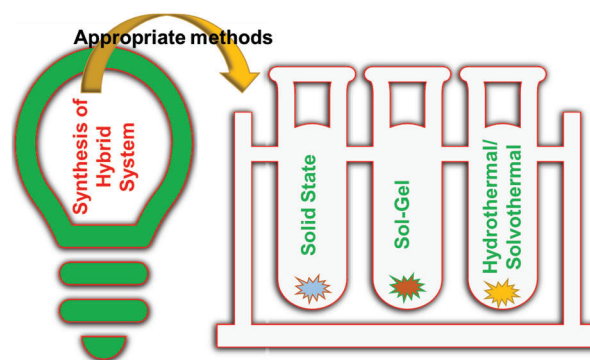


Figure 14. Most suitable method of SC-based hybrid nanoparticles.

co-doped SrTiO₃ are well situated for the feasibility of hydrogen production concerning the without-doped system.^[90] Significant decreases in the band gap of co-doped NaTaO₃ with C-S, N-N, and N-P were also reported but can only work as an electrode for reducing water in place of oxidation.

On the other hand, apart from this discussion, hybrid SC photocatalysts can be obtained with suitable and tunable properties by using some synthesis methods. These synthesis methods are shown in Figure 14.

6. Applications of Hybrid SC Photocatalyst Nanomaterials

As we know that hybrid SC nanomaterial that acts as photocatalyst can be made by the combination of metals, non-metals and metalloids with a particular SC.^[18] They perform the act of photocatalysis and play a significant role in various applications like conversion and storage of energy, environmental techniques such as air and water treatment, etc.^[91] Besides this, these hybrid SC photocatalysts play an essential role in artificial photosynthesis, hydrogen production, wastewater treatment, soil remediation, biomedical detection, imaging, sensing, printing, and many more.^[23] Due to its appropriate band gap and higher chemical and thermal durability with excellent photocatalytic activity, indium vanadate (InVO₄) is an outstanding SC-based photocatalyst for energy and environmental applications. However, the less use of solar energy of InVO₄ material makes its further advancement, primarily because of the slow segregation and movement kinetics of charge carriers. A different application of InVO₄ catalysts is shown in Figure 15a with its various forms. Generally, on behalf of band alignments and mechanism behind carrier transfer, the heterojunction-based photocatalyst's configuration could be categorized into five types: Type I system (maintains the straddling gap), Type II system (maintains the alternate gap), Z-scheme system (keeps the alternate gap), Type III system (maintains the broken gap), and Schottky junction system (Figure 15b).^[92]

Some applications, like energy and environmental applications, are discussed in the next section in detail.

6.1. Energy Applications

As we know that the need of energy is increasing day by day as it is the basic thing that fulfills the daily basic needs of human

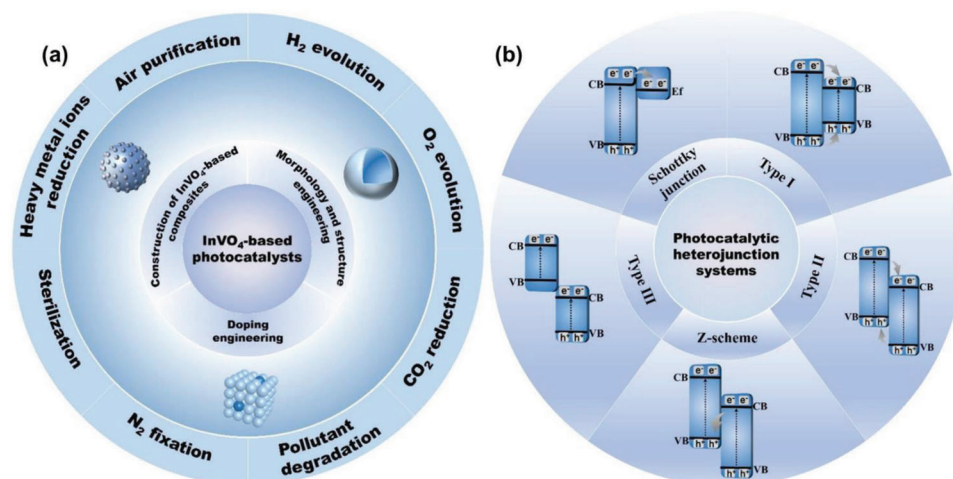


Figure 15. a) Various environmental applications of the InVO₄-based catalyst. b) Graphic design of the band arrangements and transporter transfer ways of the several kinds of heterojunctions. Reproduced with permission.^[92] Copyright 2022, Elsevier.

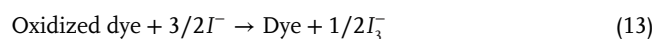
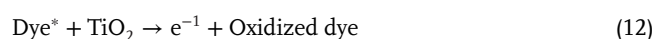
beings. Conventional energy sources are very few, so we need alternative energy sources. The energy sources must be cost-effective and eco-friendly in nature. For this purpose, solar energy is a suitable option. But this also has some challenges, which is overcome by using hybrid SC nanomaterials as photocatalyst.^[93] Moving towards the era of rapid advancement, improving the exactness and competency of experimental and theoretically used methods is necessary. The large amount of data obtained from material science fields required standard and data-based scientific research.^[94] Further, to solve the problem related to energy production, photocatalysis, electrocatalysis, and photoelectrocatalysis provide an advanced platform for sustainable energy conversion. Recently nanomaterials based on multi-component emerged as suitable materials in photocatalysis. These multi-components, when coming together, increase the synergistic effect to overcome all the limitations. These multi-component systems are also cost-effective as they do not include noble metals.^[95] The applications of photocatalysis are much more; let us discuss some in detail.

6.1.1. Photovoltaic Solar Cell

A device that converts the sun's solar energy into electrical energy is a solar cell or photovoltaic cell (PVC). This is an eco-friendly technique to produce energy. This technique's prime and most important agenda is to economically increase solar cell efficiency,^[96] as we all know that crystalline silicon in the form of thick single and multi-junction structures is used in PVC. There are many commercially used PVCs known in which, InGaAsN-based solar cells had more efficiency of 30% as compared to single-junction Si-cells (13%) and multiple-junction GaInP₂/GaAs-based solar cells (27%).^[23] Moreover, these devices have some limitations, like higher production costs and difficulty synthesizing materials. The p-n junction-based SC diodes are used to prepare Si-based solar cells. In this, an in-built electrical field is present, which helps to separate electrons and holes generated utilizing sunlight and finally stored as electric current.

CdTe, GaAs, CuInSe, etc. are also used to make solar cells in place of Si. They perform better than Si but are very costly. Si-based solar cells are also little in use due to their high cost and the poisonous chemical used in their preparation. So, we need less harmful cheap materials. These nanostructured hybrid materials have a large surface area with improved properties and are used to make lightweight PVC.^[97]

On behalf of these hybrid nanomaterials, two types of PVCs are known; 1) Dye-sensitized solar cell (DSSC), 2) Quantum dot solar cell (QDSC). In the case of DSSC, the dye particles adsorbed over the surface of NPs. Firstly, a DSSC based on a TiO₂ SC is prepared, in which a 10 μm thick film of TiO₂ was used that was coated with a layer of charge transfer dye, i.e., N₃ dye. When the cell receives sunlight, the dye molecules photoexcited; as a result, electrons come out from the TiO₂ conduction band. This exhibited high converting efficiency of the sun into electricity, i.e., more than 80%.^[98] Further research is going on to use QDs based on inorganic SCs in PVCs, in which QDs replace organic dye molecules. These QDs are a sensitizer for metal oxide NPs having more significant band gaps. QDs are used thermally more stable and color-tunable, hence controlling the shape and size of NPs. These types of PVCs consist of two components, i.e., metal oxide (like TiO₂) as a SC and sensitizers (like dye, polymer, QDs, etc.). The reactions that take place during energy production in DSSC are shown in Equations (11–14) as^[99]:



In another study, a hybrid SC Au@TiO₂ core-shell is taken; the surface of this material was decorated with CdS NPs and formed an Au@TiO₂-CdS structure. This fabricated ternary material created a way in the interior side to transfer electrons excited by the

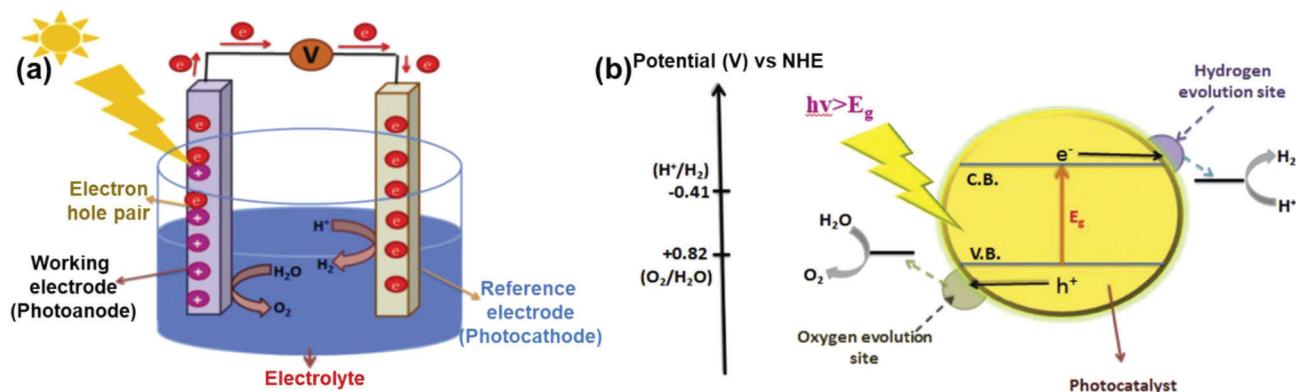


Figure 16. a) Pictorial representation, and b) a simple working mechanism of the photoelectrochemical cell. Reprinted with permission.^[106] Copyright 2018, Elsevier.

visible light from CdS. Electrons move toward the core Au by using the bridge of TiO₂, i.e., CdS→TiO₂→Au. Au NPs are not entirely covered by TiO₂ and hence work as internal co-catalyst and help in hydrogen production via the reduction of protons.

Further, a near-IR absorbing solar cell was developed by some researchers that are highly transparent to visible light with 1.7% ± 0.1% power conversion efficiency and >55% ± 2% visible transmission. The excitonic property of organic SCs to give photovoltaic architectures is not obtained via inorganic SCs. By the alignment of the active layer absorption selectively in the near-IR, researchers can enhance the architecture by using a reflector for near-IR that is made up of a DBR mirror positioned at 800 nm that gives a transparent solar cell efficiency approaching that of the non-transparent control cell. Finally, these photovoltaic solar cells offer a guide for attaining higher proficiency and higher transparency photovoltaic cells that can be used in windows to produce power, reduce the cost of cooling, and scavenge energy.^[100] Several nanocrystals based on SCs are used to fabricate photovoltaic cells; these include Cu₂S, CdS, PbS, Cu₂ZnSnS₄, CdSe, PbSe, etc. In this manner, a CdSe/CdTe NRs-based bilayer was fabricated using photovoltaic devices. The photoconversion process of this layer is based on the donor-acceptor process, in which photo excitations experience an energy-driving force for the transfer of charge. On the other hand, the separation of electrons and holes occurs at the interface. The cell shows an open circuit voltage of 0.41 V and a short circuit current of 0.58 mA cm⁻².^[101] The solar cells based on the Schottky junction also pay attention because of an energy barrier at the interface of SC-metal. It can separate of the photogenerated carrier. In this manner, using a layer-by-layer deposition approach, a PVC based on PbSe nanocrystals over an indium tin oxide glass substrate. The cell has a large short-circuit photocurrent of >21 mA cm⁻².^[102]

Further, high-density CdS nanowires (CdSNW) were fabricated over a glass substrate coated with fluorine-doped tin oxide using the vapour-liquid-solid process. For this process, approximate temperature maintained is 450 °C. In combination with poly[2-methoxy-5-(2'-ethylhexyloxy)-1,4-phenylenevinylene (MEH-PPV), CdSNW forms a hybrid structure MEH-PPV/CdS. This material absorbs and emits UV-vis light and is used in the photovoltaic cell.^[103] For next-generation photovoltaic solar cells,

which are ultrathin and very effective, 2D materials are a good candidate. Bouziani et al.^[104] fabricated a S-based material for solar cell technology, i.e., Janus monolayer of tin monochalcogenides. This material consists of Janus Sn₂SSe (type TA) and Janus SnGeS₂ (type TB) nanosheets. These materials are good solar energy absorbers with exemplary electronic and optical behavior. The photovoltaic efficiency of single-junction solar cells of SnGeS₂ is 27.47% and for Sn₂SSe is 28.12%.

6.1.2. Photoelectrochemical and Photocatalytic Hydrogen Production by Splitting of Water

A photoelectrochemical (PEC) cell is a device that converts light energy into chemical energy. This chemical energy is stored in some molecules like H₂ by electrochemical reactions, e.g., the water splitting.^[105] The PEC cell consists of a cathode, anode electrodes, and an electrolyte. The redox reactions and transfer of electrons take place over these electrodes. For many years, the PEC anode has been known as a photoanode and is made of SCs, while the cathode is made from Pt. Both electrodes are immersed in an electrolyte. PEC's simple representation and working are shown in **Figure 16a,b**. When photon energy equal to or greater than the bandgap of SCs is incident on the anode, the electrons of the valence band get promoted into an empty CB due to excitation. These electrons are now transferred to the cathode and react with the proton to form hydrogen, while holes present at the photoanode react with water to form oxygen.^[106]

In most cases, to perform the former reaction, the potential is applied from outside, known as the photoelectrochemical process. If photooxidation and photoreduction take place on photoelectrode or the same material without providing any external potential is known as photochemical. These processes also use some catalysts and are known as photocatalytic processes. Water production is done via the splitting of water using a photoelectrochemical and photocatalytic mechanism. Hydrogen is a clean and renewable source of energy. SCs with particular properties can enhance the solar water splitting to get H₂. A group of SCs known as ferrites having formula MFe₂O₄ make possible solar hydrogen production. It was investigated that hydrogen can be obtained by water splitting using a [Pt]/Na₂SO₄ (0.1 M)

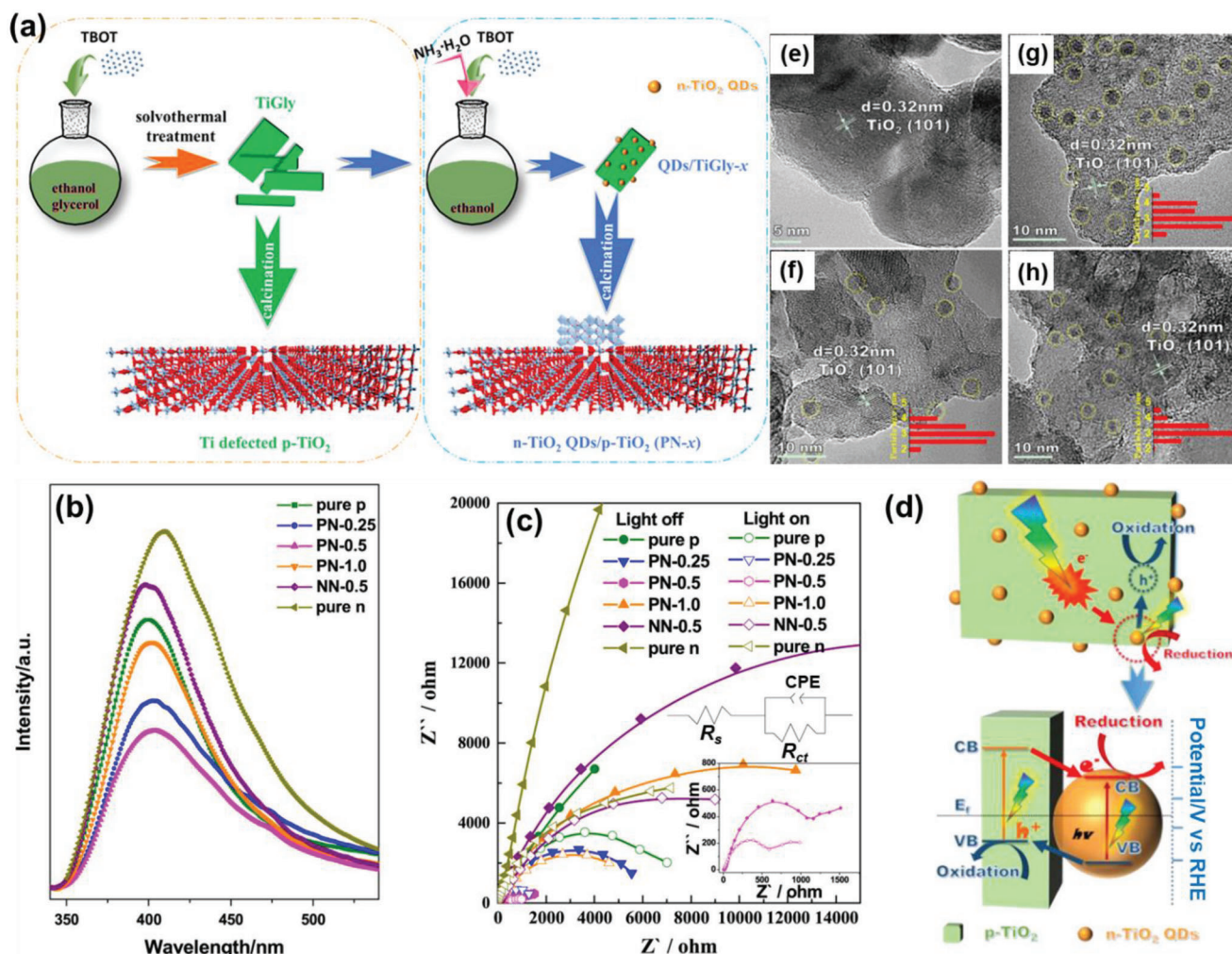


Figure 17. a) A synthetic method for fabrication of p-type TiO_2 with p-n homojunction of TiO_2 b) PL steady-state spectra and c) EIS plots for p-type TiO_2 , n-type TiO_2 , PN-x, and NN-0.5, and the inset in (c) is the enlarged plots for PN-0.5; d) representation of the transfer of charge and its separation in p-n homojunction. TEM images of pure p-type TiO_2 e); PN-0.25 f); PN-0.5 g); PN-1.0 h). The insets of (g, h) are the size distribution for TiO_2 QDs. Reprinted with permission.^[108] Copyright 2016, Elsevier.

$|\text{p-CaFe}_2\text{O}_4|$ PEC. This water splitting is induced by visible light. Photocathodes are prepared using a pulsed laser deposition approach in which a thin layer of CaFe_2O_4 is deposited over a glass covered with fluorine-doped tin oxide. Under the irradiation of visible light of (300 W Xe), approx. $4.8 \mu\text{mol m}^{-2}\text{h}^{-1}$ hydrogen is produced.^[107]

Further, it was observed that by making a junction between SCs PEC and photocatalytic H_2 , production is improved due to enhanced charge separation. For this purpose, p-n homojunction is the efficient arrangement. Some researchers investigate a TiO_2 -based p-n homojunction via depositing n-type QDs of oxygen-defected TiO_2 over a p-type TiO_2 titanium-defected surface. The fabrication of p-type TiO_2 and TiO_2 p-n homojunction is shown in Figure 17a.

The efficiency of charge separation and charge transfer of p-n homojunction is higher than others, hence having higher photoactivity as shown by PL and electrochemical impedance spectroscopy (EIS) (Figure 17b,c). This shows the higher performance

of fivefold in PEC and 1.7-fold photocatalytic hydrogen generation compared to p- TiO_2 . Further, the separation of charge and its transfer in the p-n homojunction of TiO_2 is shown in Figure 17d. The TEM image of the p- TiO_2 sheet in its purest form is shown in Figure 17e, which shows its crystalline and clean surface. The TiO_2 p-n homojunction is known as PN-x ($x = 0, 0.25, 0.5$, or 1.0 mL of Tetra butyl titanate (TBOT)). Figure 17f-h shows PN-x for nanosheets of p-type TiO_2 that were obtained from the breakdown of TiGly, which shows PN-0.25 in Figure 17f, PN-0.5 in Figure 17g and PN-1.0 in Figure 17h. The dark and contrast particles are the crystallized form of TiO_2 QDs, which is very similar to most of the particle sizes of ca. 3 nm, as shown in the inset of Figure 17f-h.^[108]

Further, it was reported that plasmonic-metal/two-dimensional SC nanocomposites are used in photocatalysis and hence valuable for the photocatalytic water splitting to produce hydrogen.^[109] With a suitable bandgap of 2.37 eV, BiVO_4 is a promising n-type SC photocatalyst for the photoelectrochemical

water splitting to produce hydrogen. BiO_4 act as a photoanode, absorbing approximately 10% of solar energy and creating 7.5 mA cm^{-2} of maximum photocurrent.^[110] Hydrogen is a clean energy source or fuel produced by solar water splitting. In this process, the solar energy directly stores in the chemical bonds. SC-based materials are required for photoelectrochemical devices that catalytically change photons into chemical energy.^[111] For this purpose, many changes are done in SCs, such as doping cations or anions, alloy formation, composite fabrication, etc. These procedures make SCs more efficient photocatalysts for harvesting solar energy up to the maximum. Furthermore, advancements in new engineering methods introduced co-catalyst, dye-sensitizers, and QDs into SCs to enhance their photocatalytic efficiency and, hence, hydrogen generation.^[112] The balanced preparation of an effective heterojunction is not easy to improve activity related to the photocatalytic evolution of hydrogen.^[113] Further, to replace the traditionally used fossil fuel, H_2 is the most suitable and eco-friendly candidate with its high calorific value.^[114] For the catalytic generation of H_2 , a heterojunction $\text{Mn}_{0.2}\text{Cd}_{0.8}\text{S}$ -diethylenetriamine/porous $\text{g-C}_3\text{N}_4$ was fabricated that enhances the transfer of charge at the interface and hence provides electron for photocatalytic H_2 production.^[115]

In addition to this, for the photocatalytic production of H_2 from the water splitting, colloidal Au-ZnSe hybrid NRs are synthesized. Density functional theory (DFT) calculations show that the tips of Au on ZnSe hybrid NRs gain more adsorption of hydrogen in comparison to pristine Au. The H_2 production rate of this hybrid is $437.8 \text{ } \mu\text{mol h}^{-1} \text{ g}^{-1}$.^[116] Using the hydrothermal approach, a heterostructure is fabricated based on a nanosheet of MoS_2 coated with nanobelt of TiO_2 , i.e., $\text{TiO}_2@\text{MoS}_2$ with 3D configuration. The as-prepared catalyst shows great performance toward the photocatalytic production of H_2 without using noble metals. In addition, the as-prepared heterojunction $\text{TiO}_2@\text{MoS}_2$ shows excellent performance toward adsorption and photocatalytic degradation of dyes present in polluted water.^[117] A heterojunction CdS nanorod/oxygen-terminated $\text{Ti}_3\text{C}_2\text{T}_x$ MXene nanosheet was fabricated, showing higher catalytic hydrogen evolution. The CdS used 1D in nanorod form, and MXene was used in 2D nanosheet form. This higher rate of hydrogen evolution is due to the terminally present group that contains oxygen at the surface of $\text{Ti}_3\text{C}_2\text{T}_x$ MXene that extends the absorption of light spectra and intimate Schottky contact and hence increases the transfer of charge at the interface. This results in the photocatalytic production of hydrogen for a long time.^[118]

As we know that by using solar energy production of hydrogen takes place by photocatalytic and photoelectrochemical water splitting. For this purpose, the minimum band gap should be 1.23 eV .^[53] A 2D/2D/2D layered heterojunction that worked as a photocatalyst is fabricated with coupling interfaces. To confirm the CdS/ WO_3 (2D layered) step-scheme heterojunction and the ohmic junction of CdS/MX, UV photoelectron spectroscopy, electron spin resonance spectroscopy, and X-ray photoelectron spectroscopy were done. The material shows excellent performance toward the production of hydrogen.^[119]

A new hollow cubic-shaped CoS is obtained from Co-ZIF-9, and the S-C bond is positively created between the CoS and $\text{g-C}_3\text{N}_4$. The constructed S-C bond works like a connection for electronic transmission that allows the fast transfer of photoelectrons

toward the active site for hydrogen evolution in CoS. On the other hand, the outcomes obtained from EIS and time-resolved PL spectroscopy show that the S-C bond also works like a bridge that transfers photogenerated carriers quickly in the composite material and hence attains the consequence of higher-competence hydrogen generation. The hydrogen production rate of SgZ-45 is $9545 \text{ } \mu\text{mol g}^{-1}$ in 5 h, which is 53 and 12 times greater than that of $\text{g-C}_3\text{N}_4$ and ZIF-9, respectively. The intrinsic mechanism of photoelectron transfer via S-C bonds can be confirmed using DFT calculations.^[120]

By using the one-step hydrothermal route, a dual co-catalyst $\text{Ni}_2\text{P-NiS}$ was fabricated. After that, this co-catalyst combined with nanosheets of gC_3N_4 gives $\text{Ni}_2\text{P-NiS/gC}_3\text{N}_4$ heterojunction. Further results show that the material shows a higher rate of H_2 production, i.e., $6892 \text{ } \mu\text{mol g}^{-1} \text{ h}^{-1}$. This rate is 46.1 times greater than gC_3N_4 , which is $150 \text{ } \mu\text{mol g}^{-1} \text{ h}^{-1}$, 7.5 times greater than 15% $\text{NiS/gC}_3\text{N}_4$, which is $914.5 \text{ } \mu\text{mol g}^{-1} \text{ h}^{-1}$, and 4.4 times greater than 15% $\text{Ni}_2\text{P/gC}_3\text{N}_4$ which is $1565.9 \text{ } \mu\text{mol g}^{-1} \text{ h}^{-1}$.^[121] Using the solvothermal method, a 2D/2D s-scheme heterojunction composite was fabricated, i.e., $\text{Ti}_3\text{C}_2/\text{ZnIn}_2\text{S}_4$ (ZIS)/CdS modified from Ti_3C_2 (MXene). The heterojunction improves the electron-hole separation efficiency. Further, the increase in the transfer of charge 2D/2D Van der Waals gives a strong force of interaction and a large contact area. The synergistic effect of $\text{Ti}_3\text{C}_2/\text{ZIS}/\text{CdS}$ composite photocatalyst greatly accelerates hydrogen production.^[122]

Further, to enhance the photocatalytic production of hydrogen, the VB site of gC_3N_4 was connected with the CB of WO_3 by a W-N bond to form a heterojunction photocatalyst.^[123] A cheap metallic Ni_3C co-catalysts having two nanocrystals $\text{Zn}_{0.5}\text{Cd}_{0.5}\text{S}$ (ZCS) solid solution homojunction is used for hydrogen production by using visible light via a straightforward method. As-fabricated $\text{Zn}_{0.5}\text{Cd}_{0.5}\text{S-1\% Ni}_3\text{C}$ (ZCS-1) nanohybrid shows the highest photocatalytic evolution of H_2 at a rate of $783 \text{ } \mu\text{mol h}^{-1}$ in the presence of visible light, that is 2.88 times higher as compared to the nanocrystal of pristine twin ZCS solid solution.^[124]

This $\text{Au@TiO}_2\text{-CdS}$ metal-SC hybrid photocatalyst is also used in solar fuel production. The production of hydrogen is shown in Figure 18a. The absorption spectra of $\text{Au@TiO}_2\text{-CdS}$ are shown in Figure 18b. The absorption band at approximately 320 nm may be related to the anatase TiO_2 band edge absorption. The band absorption of CdS NPs is shown from 360 to 520 nm. Further, $\text{Au@TiO}_2\text{-CdS}$ was also utilized for photocatalytic hydrogen production by exposure to visible light with a wavelength greater than 420 nm. Additionally, for the comparison, pure CdS NPs and $\text{TiO}_2\text{-0.2CdS}$ were fabricated without using gold. The graph plotted as shown in Figure 18c,d shows that both the samples, i.e., pure CdS NPs ($0.25 \text{ } \mu\text{mol h}^{-1}$) and $\text{TiO}_2\text{-0.2CdS}$ ($0.28 \text{ } \mu\text{mol h}^{-1}$), show poor photocatalytic performance for the production of hydrogen.^[125]

Despite this, some other materials like Conjugated covalent organic frameworks (COFs) also act as photocatalysts for the production of H_2 due to their higher crystallinity, larger surface area, and different structure. On the other hand, the charge separation power of COFs is not good.^[126] So, it was concluded that materials that exhibited a higher ability of charge separation and their easy transport act as good photocatalytic materials for hydrogen production from water splitting.

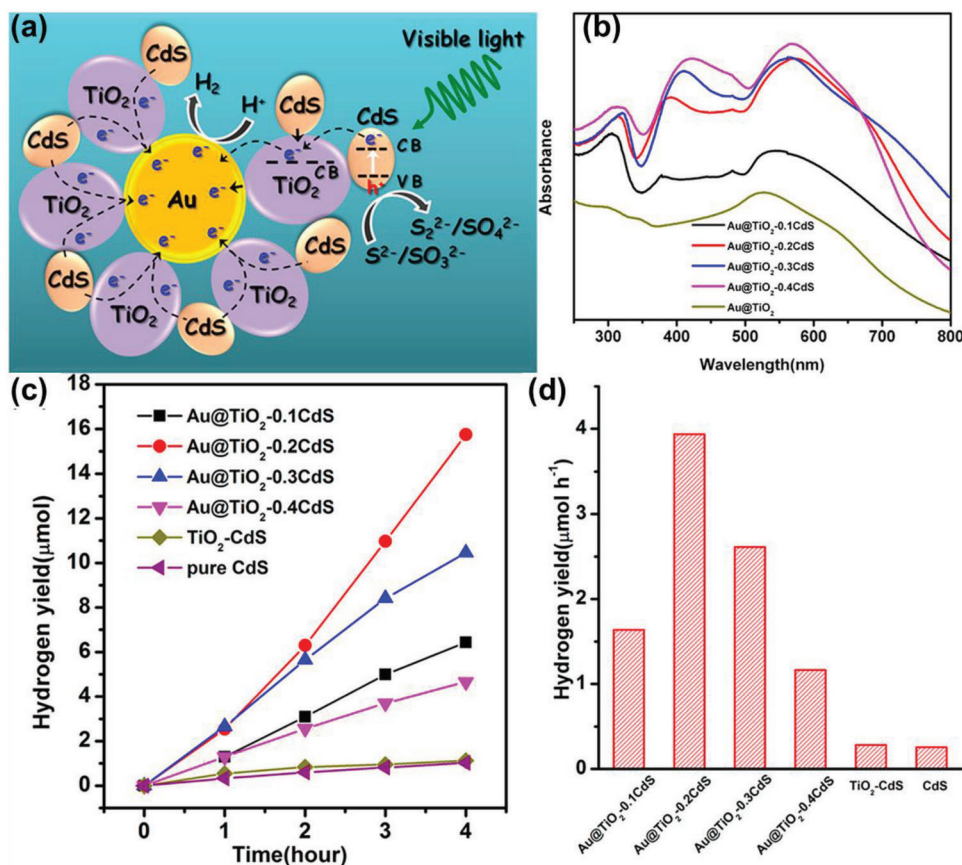


Figure 18. a) Schematic illustration of photocatalytic H₂ generation by Au@TiO₂-CdS ternary nanostructures under visible light irradiation. b) Different samples of Au@TiO₂-CdS showing UV-vis diffuse reflectance spectrum. c) Curves of the photocatalytic evolution amount of H₂ versus visible-light-exposure ($\lambda > 420$ nm) time by different samples. d) Graph showing various sample's evolution rate of H₂-gas. Reprinted with permission.^[125] Copyright 2013, American Chemical Society.

6.1.3. Photo-Assisted Direct Alcohol Fuel Cell

Among the differently used technology, the fuel cell is the predominant candidate that convert chemical energy of fuel combustion directly into electrical energy without causing environmental pollution.^[127] Further, a Pt-Ru-based bimetallic catalyst^[128] was fabricated for the working of a direct methanol fuel cell (DMFC) efficiently, which was based on carbon support.^[129] The Pt/C commercially available cathode is separated by Pt-Ru/C based anode by a proton exchange membrane (PEM). This PEM allows the transport of ions between the two compartments of the fuel cell. But this catalyst had some limitations like high cost of metal and poisoning by CO, due to which activity as well as efficiency of fuel cell affected and leads the high price of DMFC.

To overcome these problems, many changes were made, like an alloy of Pt with other metals, i.e., Pt-M, the use of Pd in place of Pt,^[130] and the introduction of oxophilic metals like Au for enhancement of CO tolerance,^[131] etc. But there are some limited researches in which hybrid SC nanomaterials like Pt/TiO₂/C are used to enhance the efficiency of DMFC. Further, it was reported that when TiO₂ SC is combined with Pt metal, it efficiently increases the surface area and fuel cell activity. This enhanced fuel cell performance is due to the interaction of TiO₂ with Pt, which leads to changes in the electron density of Pt d-orbital.^[132] Fur-

ther, a report discussed the irradiation effect on TiO₂/Pt-Ru. According to this report with Pt-Ru electrocatalyst, the nanoparticles of TiO₂ were also introduced in the electrode for electrooxidation of methanol photo-catalytically and electrocatalytically. It was found that the current produced is increased by 30%, hence the power output by introducing TiO₂ NPs in photocatalytic oxidation of methanol during irradiation of UV light.^[133]

Further, a Pt-TiO₂ hybrid electrode was developed by Lin et al.^[134] by using the photo-deposition approach in which ethylene glycol is used as a reducing agent. When a comparison was made among various electrodes, i.e., with Pt-thin film, Pt-NPs and Pt-TiO₂ for UV-boosted methanol oxidation, it was found that the highest increase in current up to 48% for 100 W illumination and 9% for 4 W illumination was observed in case of Pt-TiO₂ electrode. This result is due to a decrease in illumination light shielding by the Pt-TiO₂ junction, increasing the potential of Photo-assisted fuel cells. Recent researches indicate that by using the optical performance of hybrid SCs nanoparticles as an electrocatalyst by irradiation of light, the electrocatalytic performance and stability of the electrode can be significantly enhanced. The working of the photo-assisted fuel cell is shown in Figure 19.^[135] The behavior of different hybrid photocatalysts toward alcohol oxidation reactions with dark and light conditions is shown in Table 2.

Table 2. Current updates of electrocatalytic behavior of alcohol oxidation reactions with different hybrid SCs as photocatalysts in dark and light.

Catalyst	Analyte	I_{light}	I_{dark}	$I_{\text{light}}/I_{\text{dark}}$	Reference
Pt-Ru/TiO ₂ /carbon fiber	MeOH	45.0 mA cm ⁻²	23.3 mA cm ⁻²	1.93	[133]
Pt/rGO/TiO ₂ /carbon fiber	MeOH	507 mA mg ^{-e}	364 mA mg ⁻¹	1.39	[136]
Pt/CdS/FTO	MeOH	8.64 mA cm ⁻²	3.60 mA cm ⁻²	2.40	[137]
Pt/TiO ₂ /Vulcan XC-72R carbon	MeOH	3.29×10 ³ mA mg _{Pt} ⁻¹	1.21×10 ³ mA mg _{Pt} ⁻¹	2.71	[138]
Pt/ZnO/ketjen black	MeOH	964 mA mg _{Pt} ⁻¹	432 mA mg _{Pt} ⁻¹	2.23	[139]
PtNiRu/TiO ₂	EtOH	24.6 mA cm ⁻²	9.90 mA cm ⁻²	2.48	[140]
Au nanowires/mZnO	EtOH	1.85 mA mg _{Au} ^{-u}	0.840 mA mg _{Au} ⁻¹	2.20	[141]
Pt NPs/rGO/CdS	EtOH	3.63 mA cm ⁻²	1.12 mA cm ⁻²	3.24	[142]
Pt NPs/Titanium oxide nanotubes	Formic acid	14.4 mA cm ⁻²	10.2 mA cm ⁻²	1.41	[143]
Pd/Cu ₂ S	Ethylene glycol	3.26×10 ³ mA mg _{Pd} ⁻¹	1.89×10 ³ mA mg _{Pd} ⁻¹	1.72	[144]
Pt/BiOI	EtOH	293 mA mg _{Pt} ⁻¹	874 mA mg _{Pt} ⁻¹	2.99	[145]
Pt/graphene/TiO ₂	MeOH	4.72×10 ³ mA mg _{Pt} ⁻¹	3.36×10 ³ mA mg _{Pt} ⁻¹	1.40	[146]

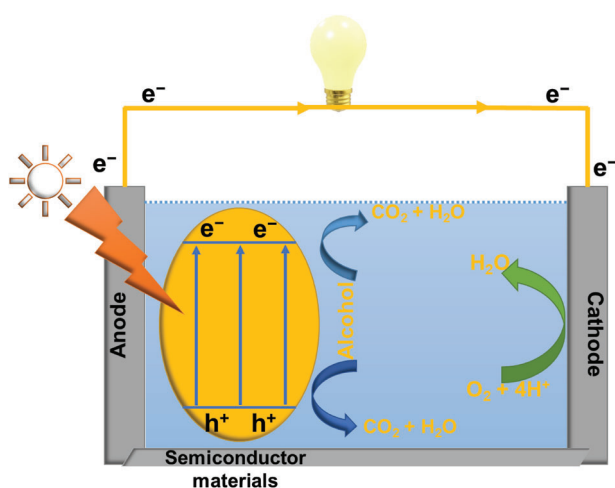


Figure 19. Photo-assisted reaction of DMFC.

An ultrasmall nanocluster of Pt was deposited over an ultrathin two-dimensional nanosheet of g-C₃N₄ using a simple reflux process. Ethanol is used as a reducing agent in this process. The TEM images of g-C₃N₄ nanosheets (**Figure 20a**) and Pt/g-C₃N₄ modified electrode (**Figure 20b**) show the approximate size of Pt nanocluster is 3.2 nm. When the irradiation of visible light occurs on the material, Pt/g-C₃N₄ modified electrode shows great activity toward oxidation of methanol. So, by incorporating Pt, the catalytic activity and stability of the SC photocatalyst increase. The given pathway for the strong methanol oxidation reaction by the as-prepared material is shown in **Figure 20c**. As represented by **Figure 20d**, the cyclic voltammetry (CV) was -0.1 V to 0.2 V in a KOH solution (1 M) saturated by nitrogen. The cathodic peak was obtained at -1.0 V from hydrogen adsorption and the anodic peak at -0.6 V versus SCE from hydrogen desorption. It is also clear from the CV that the integrated area of the peak for Pt/g-C₃N₄ is more significant than PtNPs. The electrochemical active surface area for Pt/g-C₃N₄ is 12.87 cm² mg⁻¹, and for PtNPs is 10.58 cm² mg⁻¹.

Figure 20e represents the linear sweep voltammetry (LSV) of bare Pt NPs and modified electrode of Pt/g-C₃N₄ under the situation of dark and irradiation to light in MeOH (1 M) and KOH (1 M) solution. The onset potential of Pt/g-C₃N₄ shifts more negatively on light exposure compared to dark situations. At a potential of -0.3 V, the current density of the modified electrode of Pt/g-C₃N₄ under light exposure is 132 mA mg⁻¹, which is very high compared to a dark situation of 56.0 mA mg⁻¹. The current density for pure Pt NPs is significantly lower, i.e., 42.3 mA mg⁻¹. This behavior Pt/g-C₃N₄ acts as a promising photocatalyst with increased active surface area. The CV explained this (**Figure 20(f)**), showing the activity of Pt/g-C₃N₄ in different conditions, i.e., curve (i) in the dark, curve (ii) with exposure to visible light and curve (iii) for pure Pt NPs. The highest performance was observed with the incorporation of Pt and exposure to visible light.^[135]

6.2. Environmental Applications

For the removal of organic contaminants present in the environment, photocatalytic oxidation is a good method. Photocatalytic oxidation can remove all the organic contaminants efficiently compared to other methods like chemical oxidation, adsorption, biodegradation, etc., and are eco-friendly. Photocatalytic oxidation with visible light is the most efficient and is frequently used because 43% of solar energy consists of visible light and is easily accessible. Many photocatalysts are known for the oxidation that works on visible light; these are Bi₂O₃, MoS₂, Bi₂WO₃, WO₃, CdS, Fe₂O₃, g-C₃N₄, etc.^[148] Using the precipitation method, a composite was fabricated, i.e., Ag₃PO₄/C₃N₄ with particles of Ag₃PO₄ and a hollow nanosphere of C₃N₄. This composite produces oxygen at a higher rate of 803.31 μmol g⁻¹ h⁻¹.^[149] The process related to this photocatalyst for environmental remediation is discussed in detail in the next section.^[150] The photocatalyst's mechanism for water remediation is shown in **Figure 21**.

6.2.1. Water Purification

The easy accessibility of fresh and pure drinking water is a much important aspect of our society. This also determines the health

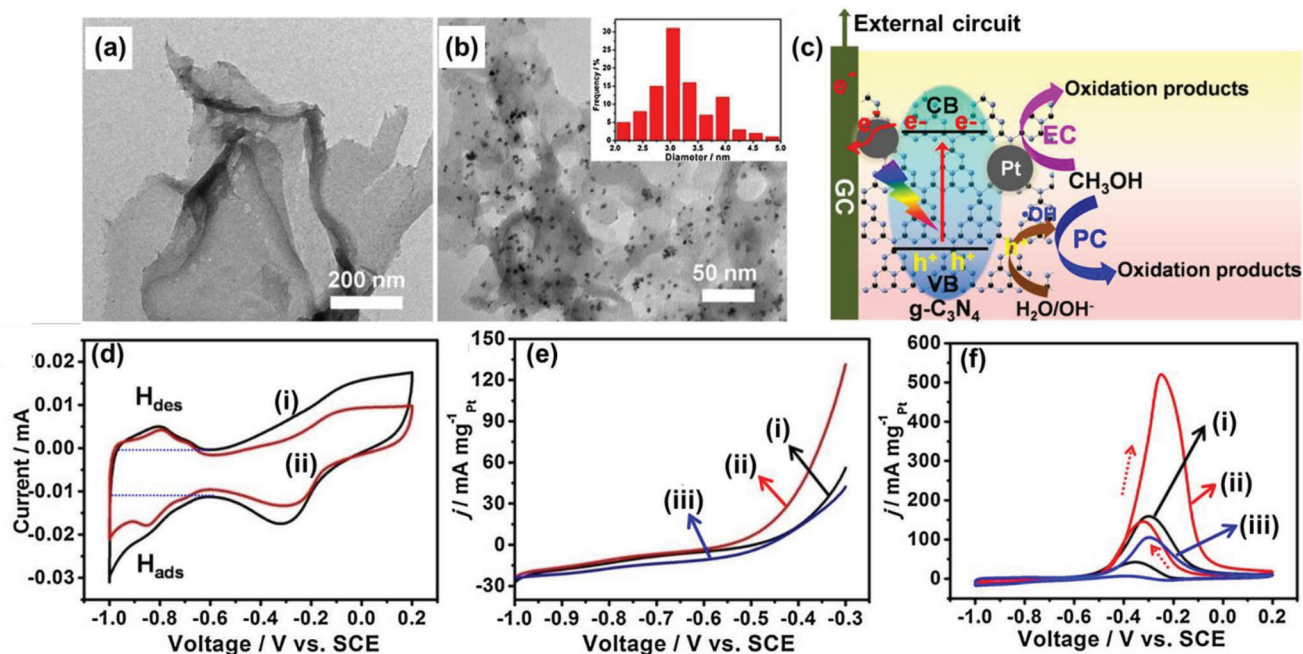


Figure 20. a) TEM picture of ultrathin $g\text{-C}_3\text{N}_4$ nanosheets. b) TEM image of Pt/ $g\text{-C}_3\text{N}_4$ nanocomposites. c) Pictorial representation for the synergistic electrocatalytic and photocatalytic-based methanol oxidation reaction by using the modified electrode of Pt/ $g\text{-C}_3\text{N}_4$ on exposure to visible light. d) CVs of the Pt/ $g\text{-C}_3\text{N}_4$ (i) and pure Pt NPs (ii) modified electrode in KOH (1 M) solution over a scan rate of 50 mV s^{-1} . LSV e) and the 170th CVs f) CV of the Pt/ $g\text{-C}_3\text{N}_4$ in the absence of sunlight (i) and visible light irradiation (ii), and Pt NPs in pure form (iii) in a mixture of KOH (1 M) and CH_3OH (1 M). Reprinted with permission.^[147] Copyright 2017, Elsevier.

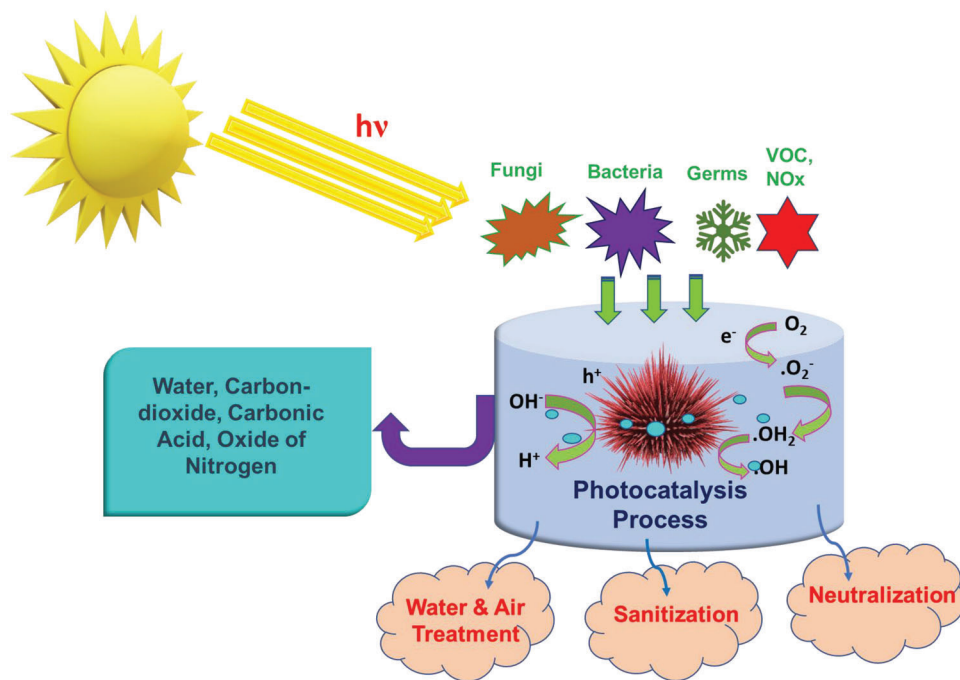


Figure 21. Representation of photocatalysis for wastewater treatment.

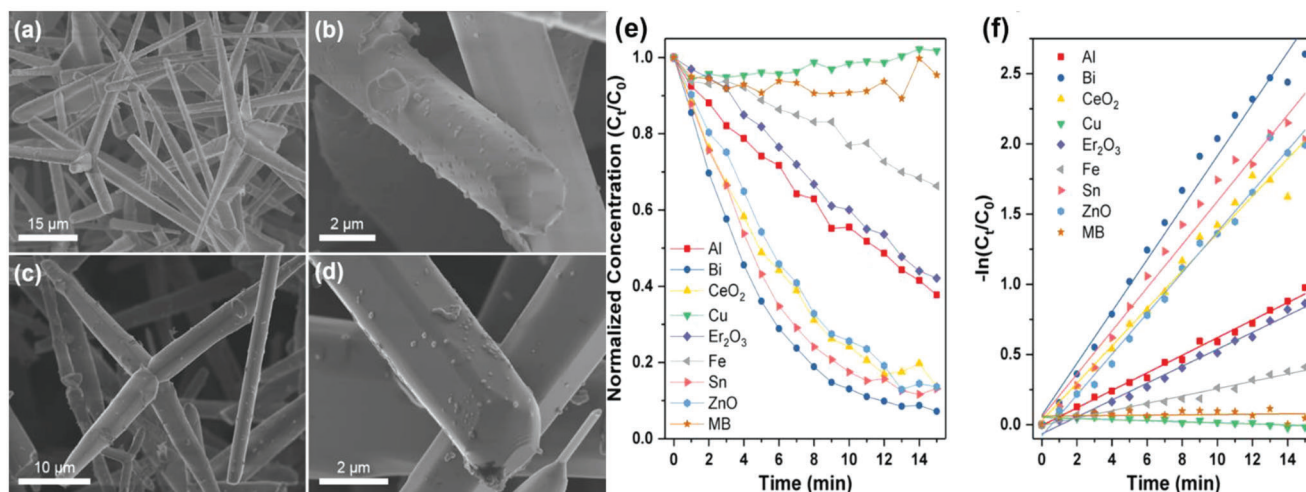


Figure 22. SEM of hybrid ZnO-T ceramic networks at less followed by higher magnifications: (a,b) with CeO_2 , and (c,d) with Er_2O_3 . e) Photocatalytic breakdown of MB dye in the presence of various metal oxide hybridized ZnO-T ceramic arrangements. f) MB photocatalytic degradation by First-order kinetics and plotted it by transforming it into linear curves. Reprinted with permission.^[157] Copyright 2017, Elsevier.

of humans and animals. As we all know, the increase in industrialization releases a large amount of wastewater into the environment. Despite this, agriculture also releases wastewater daily. This wastewater contains many hazardous organic and inorganic materials, chemicals, and bacteria that cause water pollution.^[151] To improve the quality of water and save the world from contaminated water, researchers will continuously develop many wastewater treatment technology. These techniques remove impurities from water, i.e., chemicals and biological pollutants.^[152] The ancient technologies are insufficient to remove secondary pollutants from the water. To improve the water quality and remove the secondary pollutants or chemicals present in water, advanced oxidation processes are developed. These processes are generally based on producing some reactive molecules like radicals. SC-based nanomaterials are suitable for wastewater treatment due to their large surface area, more reactivity, catalytic nature, high porosity, etc.^[153] Currently, nanomaterials based on photocatalytic degradation are used frequently and are very effective for wastewater treatment. Some suitable modifications are done to increase the photocatalytic activity of these nanomaterials.^[154] Some resourceful biological assemblies have very competent solar light absorption, matter transmission, and natural photocatalytic characteristics, like leaves, algae, sunflowers, seaweeds, bacteria, etc.^[155]

On the other hand, hybrid SC nanomaterials are used as adsorbates for pollutants. A ternary nanostructured metal-SC hybrid photocatalyst consisting of $\text{ZnO}/\text{TiO}_2/\text{Au}$ was reported by Mukhopadhyay et al.^[156] and showed higher solar adsorption. This is due to the coupling between surface-enhanced plasmonic absorption of SCs and metal excitons. This material, i.e., $\text{ZnO}/\text{TiO}_2/\text{Au}$, is used for the photocatalytic breakdown of organic pollutants present in wastewater. Using the flame transport synthesis method, 3D-ZnO ceramic nano and microtetrapods were fabricated, i.e., ZnO-Ts. The photocatalytic behavior of material based on the breakdown of methylene blue dye. Further this ZnO-Ts combined with CeO_2 , CuO , Bi_2O_3 , $\text{Fe}_2\text{O}_3/\text{ZnFe}_2\text{O}_4$, etc. The scanning electron microscopy (SEM) images of ma-

terial shown in **Figure 22a,b** with magnification for CeO_2 and **Figure 22c,d** for Er_2O_3 shows particles ranging from 10 to 150 μm . As a time, function, the degradation of methylene blue with its photocatalytic activity is shown in **Figure 22e**. The photocatalytic degradation of methylene blue dye is more in the case of hybrid ceramics materials over a while of 15 min. **Figure 22f** shows the photocatalytic breakdown of methylene blue, which is represented by pseudo-first-order kinetics. The value of constant rate k plotted in linear slope shows that the photocatalytic efficiency of ZnO-T- Bi_2O_3 hybrid shows the higher photocatalytic breakdown of MB with 27% higher rate constant as compared to bare ZnO-T ceramics.^[157]

Using the in-situ deposition precipitation method, the phosphorous and sulfur co-doped graphitic carbon nitride (PSGCN) was added with particles of AgBr, i.e., AgBr/PSGCN-100). The hybrid photocatalyst AgBr/PSGCN-100 is a heterojunction material used to degrade the Ibuprofen chemical in industrial wastewater. This catalyst is given a response to visible light. When exposed to visible light, 0.1 g of material is photodegraded 0.5 mg L^{-1} ibuprofen in 20 min, 1.0 mg L^{-1} in 30 min, and 5 mg L^{-1} in less than 60 min. Hence one can say that AgBr/PSGCN-100 is a very effective photocatalyst for the degradation of ibuprofen chemical.^[158] Further research has been going on over decades to fabricate new photocatalytic hybrid nanomaterials based on SCs. They are helpful in wastewater treatment. Moreover, sulfides and oxides of metal are also used to design these mixed materials that enhance the photocatalytic performance of SCs. By growing 0D nanodots of Bi_2WO_6 over 2D nanosheets of C_3N_5 , a 2D/0D heterojunction, i.e., $\text{C}_3\text{N}_5/\text{Bi}_2\text{WO}_6$, was prepared that was used to remove Cr (VI) and tetracycline from water by using visible light. The results show that $\text{C}_3\text{N}_5/\text{Bi}_2\text{WO}_6$ exhibited excellent performance for removing Cr (VI) and tetracycline in visible light due to strong interaction between nanodots and nanosheets of Bi_2WO_6 and C_3N_5 , respectively.^[159]

It is noted that contaminants based on fiber-based microplastics (FMP) present in wastewater are a great issue of concern. These FMPs are added to the water from the urban sewage

textile industry and cause major human issues. To solve problems related to this, a heterojunction composite, namely Z-scheme $\text{Bi}_2\text{O}_3@\text{N-TiO}_2$, was fabricated by using solvothermal and wet-impregnation methods. $\text{Bi}_2\text{O}_3@\text{N-TiO}_2$ degraded approximately 10.23 ± 1.91 wt.% of polyethylene terephthalate (PET)-FMPs over a pH = 9, which is around 3 times higher as compared to that of over the pH 7. This PET is the major FMP present in the environment. Investigational outcomes indicate that the hydrolysis of PET-FMPs in the basic medium is the chief cause for its excellent activity. Significantly, the weight-average molecular weight, the hydrophilic, and the crystallinity of PET-FMP are the main aspects that influence the photocatalytic degradation activity of PET-FMPs.^[160]

6.2.2. Air Purification

The contaminant that spoils the air quality is known as air pollutants. These pollutants mainly contain oxides of carbon, nitrogen, and sulfur with particulate matter and volatile organic compounds. In addition to these materials, some carcinogenic hydrocarbons are also in polluted air. The sources of these pollutants are cigarette smoke, vehicle emission, industrial chimney, combustion of fossil fuel, combustion of rice straw by farmers, etc. To save life on earth, air purification is much essential. Many methods were used for air purification years ago, but they could have been more effective.^[161] For the efficient purification of air, hybrid SC photocatalysts are the more practical alternative over room temperature and suitable atmospheric pressure. The cost for the SCs is not much high, and they easily mineralize the maximum organic materials. Upon exposure to sunlight, these semiconductors absorb quanta of light known as photons and produce excited electrons with holes. They can change in hydroxyl free radical ($\text{OH}\cdot$) or superoxide free radical anion (O_2^-).

These free radicals are more reactive and mineralize the air's organic pollutants by oxidation. TiO_2 degrades sulfur oxides, nitrogen oxides, and volatile organic compounds upon illumination.^[23] By moving in this direction, some researchers investigate a most versatile hybrid SC photocatalyst, Ag/TiO_2 . This material photo-catalytically oxidizes NO gas into NO_3^- ions present as air pollutants. Further, the anatase Ag/TiO_2 photocatalyst converts NO_x in N_2 on UV and visible light irradiation. On the other hand, Ag/TiO_2 also degraded the volatile organic compounds into CO_2 and H_2O . Ag/TiO_2 also breaks down the isopropanol present in industrial air as a pollutant, purifying the air.^[162]

Zhao et al. fabricated a non-noble metal photocatalyst by depositing Bi NPs over TiO_2 . The nanocomposite BiNPs/TiO_2 is used by the visible light photocatalytic method to remove NO from the air. The material shows highly enhanced photocatalytic behavior due to plasmon-mediated activation of NPs of Bi by visible light. It leads to the transfer of electrons at the interface of materials, hence holes and electron separation. Pristine TiO_2 showed negligible performance, while enhanced activity with Bi NPs under 500 nm of visible light illumination to remove NO from the air.^[163]

Further, Ahmad et al.^[164] discussed carbon-integrated SC photocatalysts to remove the volatile organic compounds from indoor air. Carbon-based materials include activated carbon, rGO,

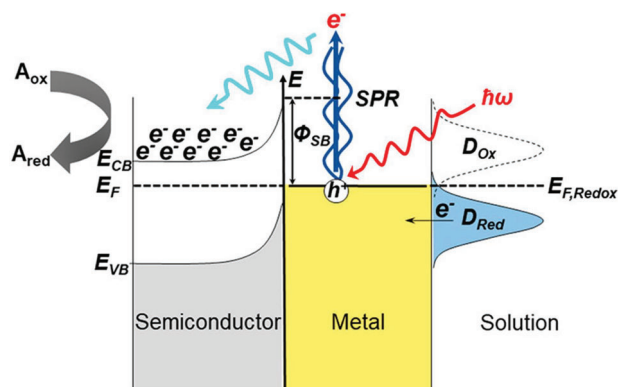


Figure 23. Schematic representation of plasmon mediated electron transfer. Reprinted with permission.^[165] Copyright 2018, American Chemical Society.

MOF, MXene, carbon QDs, $g\text{-C}_3\text{N}_4$, carbon nano-tubes, etc. They help remove volatile organic compounds due to their large surface area, optoelectronic nature, adsorption affinity, and electron transfer nature. The schematic representation of plasmon mediated electron transfer is shown in **Figure 23**.^[165]

6.2.3. Photocatalytic CO_2 Photoreduction

In recent years, there has been a growing interest in developing photocatalytic systems for reducing CO_2 into valuable chemicals using SC materials. Photocatalysis is a process that utilizes light energy to drive chemical reactions, and SC materials, such as TiO_2 and ZnO , are commonly used as photocatalysts.

One recent study by Madhusudan et al.^[166] explored using a novel heterostructure TiO_2/ZnO photocatalyst to reduce CO_2 into methanol. The researchers synthesized the photocatalyst using a sol-gel method and found that the heterostructure exhibited superior photocatalytic performance compared to pure TiO_2 or ZnO photocatalysts. The high activity was attributed to the efficient charge transfer and separation between the TiO_2 and ZnO components. Another study focused on developing a visible-light-responsive photocatalyst for CO_2 reduction.^[167] The researchers used a copper-based MOF as the photocatalyst and found it exhibited high selectivity toward producing formate ions. The MOF utilized visible light, which is more abundant in the solar spectrum than ultraviolet light, for photocatalysis.

In addition to TiO_2 , ZnO , and MOFs, other SC materials such as bismuth-based materials, copper-based materials, and cadmium sulfide (CdS) have also been investigated for photocatalytic CO_2 reduction.^[168] For instance, a recent study published in Chemical Communications reported synthesizing a bismuth vanadate (BiVO_4) photocatalyst for CO_2 reduction. The BiVO_4 exhibited high selectivity towards methane production under visible light irradiation. Overall, developing efficient photocatalytic systems for CO_2 reduction using SC materials can contribute to mitigating greenhouse gas emissions and producing sustainable fuels and chemicals. However, further research is needed to optimize the performance of these systems and address challenges such as catalyst stability and scale-up.

CO_2 in the atmosphere helps in photosynthesis, via which plants convert inorganic materials into organic food by absorbing

sunlight. On the other hand, when the amount of CO₂ increases in the atmosphere, it also causes some critical issues that are not good for human life. To overcome this problem reduction of CO₂ is required. Reduction of CO₂ into carbon feedstock using a heterogeneous photocatalyst is the most suitable method. Of specific usefulness, it is necessary to develop a photosystem capable of working in the presence of visible light, which is mainly present in sunlight, hence showing a type of artificial photosynthesis. Hybrid systems containing a metal complex and a SC are capable materials due to the excellent electrochemical and photocatalytic performance of metal complexes during the reduction of CO₂ and the capability of SCs to oxidize H₂O to molecular O₂ proficiently. The photoreduction of CO₂ using visible light is currently used to change CO₂ into a valuable energy source. Methane is the main product of this CO₂ photoreduction. But the fabrication of photocatalysts based on SCs remains a challenge.^[169]

From the above discussion, it is evident that hybrid SC-based photocatalysts are very popular for environment remediation—some of its advantages and disadvantages are discussed in brief.^[94]

Advantages of hybrid semiconductor as photocatalyst

- 1) Hybrid SCs are very economical as they are available at low cost.
- 2) They reduce air pollution by reduction of CO₂.
- 3) Photocatalysts based on hybrid SCs are non-toxic and are capable of disinfecting a range of micro-organisms in the presence of visible light.
- 4) Hybrid NPs are helpful in photocatalytic evolution of H₂ and fixation of nitrogen.
- 5) They have higher photocatalytic efficiency due to the large contact between contaminants and photocatalysts.

Disadvantages of hybrid semiconductor as photocatalyst

- 1) Lower adsorption of organic contaminants.
- 2) No proper utilization of the visible light present in sunlight.
- 3) Problem in dispersion of particles in uniform way.
- 4) Accumulation of nanoparticles takes place sometime.
- 5) The recovery of nano-sized particles is not easy.
- 6) Recombination of charge carriers, i.e., electrons and holes take place that are photogenerated in nature.
- 7) HNPs are thermally less stable in nature.

There are various hybrid SCs with diverse applications. Some of them are discussed above and summarized in **Table 3**.

7. The Appealing Directions, the Scientific Challenges, and the Reasons Behind the Poor Stability in Hybrid Semiconductor Photocatalyst Nanomaterials for Energy and Environmental Applications

7.1. Appealing Directions

Hybrid SC photocatalyst nanomaterials have emerged as a promising area of research for energy and environmental applications due to their unique properties and capabilities. These materials are composed of two or more types of SCs, each with spe-

cific properties that can be combined to improve the efficiency and performance of photocatalysis.

One of the most appealing directions in this field is the development of efficient photocatalysts for solar energy conversion. Hybrid SC photocatalysts can be used to harness solar energy and convert it into clean, renewable energy sources such as hydrogen and other fuels.^[192] These materials have the potential to play a crucial role in achieving a sustainable energy future by providing a low-cost, abundant, and environmentally friendly source of energy.

Another promising application of hybrid SC photocatalyst nanomaterials is the degradation of organic pollutants in wastewater treatment.^[193] These materials can break down organic pollutants into harmless substances through photocatalytic reactions. This process can help to purify water and reduce the harmful effects of contaminants on the environment and human health. In addition to energy and environmental applications, hybrid SC photocatalysts can also be used for other purposes, such as sterilization, air purification, and self-cleaning surfaces.^[194] These materials can be incorporated into various products and technologies to improve functionality and performance.

Researchers are exploring new approaches to further improve their efficiency and stability to advance the development of hybrid SC photocatalyst nanomaterials. One direction is to tune the composition and structure of the hybrid materials to optimize their photocatalytic properties.^[195] Another approach is to develop new methods for synthesizing and fabricating these materials, such as sol-gel, hydrothermal, and microwave-assisted methods.^[196] Overall, hybrid SC photocatalyst nanomaterials offer exciting opportunities for advancing sustainable energy and environmental technologies. With continued research and development, these materials have the potential to make significant contributions to addressing some of the most pressing global challenges of our time.

7.2. Scientific Challenges

Hybrid SC photocatalyst nanomaterials have shown great potential for energy and environmental applications, but several scientific challenges need to be addressed for their successful implementation. One of the biggest challenges in developing these materials is optimizing their photocatalytic activity. The performance of photocatalysts is strongly influenced by factors such as the composition and structure of the materials, the surface area, and the crystallinity.^[197] The challenge is to design hybrid SC photocatalysts with optimal properties that can effectively utilize solar energy to generate charge carriers and promote photocatalytic reactions.

Another challenge is the stability and durability of these materials under harsh operating conditions. For instance, photocatalysts used for water purification applications are often exposed to harsh chemical and physical environments.^[198] The materials need to be stable under these conditions to maintain their photocatalytic activity and prevent degradation over time. Another critical challenge is the development of scalable and cost-effective fabrication methods for these materials. Most existing synthesis methods for hybrid SC photocatalysts involve complex and expensive procedures.^[199] To enable their widespread use, scalable

Table 3. Different types of hybrid SCs with their properties and application.

Hybrid SCs	Fabrication approach	Characteristics	Applications	Reference
Au/CdS/TiO ₂	Hydrothermal	Shows higher photo catalytic performance on exposure to visible light	Production of solar fuels and H ₂	[125]
Au/WO ₃ /TiO ₂	Chemical deposition	Act as photocatalyst	Photovoltaic cell and environmental applications	[170]
Au/CdS/ZnS	colloidal	Highly induced by sunlight	Photocatalytic H ₂ generation	[171]
Pt/TiO ₂ /CdS	Sol-gel/irradiation	Visible light absorbing photocatalyst	Production of H ₂ and photocurrent	[172]
Pt/TiO ₂ /ZrO ₂	vacuum impregnation	Shows degradation photo catalytically	Production of H ₂	[173]
Au/CdS/ZnO	Solution-liquid-solid	Having unique structure, small size and are heterogeneous	Photocatalytic active	[174]
Pt/TiO ₂ /CuGaS ₂	Sono-chemical	Responsive to UV and visible light	Photogeneration of H ₂	[175]
Ag/TiO ₂ /Co ₃ O ₄	Anodization/photoreduction	Photochemically enhance visible light	Photovoltaic devices	[176]
Au/ α -Fe ₂ O ₃ /TiO ₂	Hydrothermal/sputtering/deposition	Act as photoanode having higher density of photocurrent	Photo electrocatalytic H ₂ O splitting and solar energy conversion	[177]
Au-Pd/TiO ₂	Chemical reduction	Enhance the visible and broad-spectrum Photocatalytic activity	photocatalytic hydrogen generation	[178]
Ag/TiO ₂ /CuO	Solution-immersion and electrodeposition	Higher -photo response to visible light	Photocatalytic breakdown of organic pollutant present in water	[179]
Au/ZnO/TiO ₂	solvothormal	Increased solar absorption	Treatment of waste water and photocatalytic splitting of H ₂ O	[156]
Pt/RuO ₂ /TiO ₂	surface modification	Act as photocatalyst	Oxidation of CO	[180]
Pd/CdS/TiO ₂	Solvothormal	Higher catalytic efficiency	Reduce poisonous Hexavalent Cr	[181]
Ag/TiO ₂ /ZnO	Electrospinning/hydrothermal/Photo-deposition p	Excellent mechanical flexibility and Good photocatalytic performance	Purification of water	[182]
Ag/TiO ₂ /CdO	Sol-gel	High photo response to UV-light	Photocatalytic breakdown of organic pollutants like methylene blue	[183]
Ag/ZnO/CuO	Chemical photochemical deposition	Superior photodegradation	Sewage of treatment	[184]
MEH-PPV/CdS	Vapor-liquid-solid	absorbs and emit UV-Visible light	photovoltaic cell	[103]
BiVO ₄	–	act as photoanode	photoelectrochemical splitting of water to produce hydrogen	[110]
TiO ₂ /Pt-Ru	–	Photochemical and electrochemical activity	electrooxidation of methanol	[133]
Pt-TiO ₂	Photo-deposition	Absorb UV light	oxidation of methanol by photo assisted fuel cell	[134]
Pt/g-C ₃ N ₄ electrode	Simple reflux	Sensitive to visible light	oxidation of methanol by photo assisted fuel cell	[135]
ZnO-Ts	Flame transport synthesis	–	photocatalytic degradation of MB dye	[157]
AgBr/PSGCN-100	In-situ deposition precipitation	Give response to visible light	Degradation of Ibuprofen chemical present in industrial waste water	[158]
Ag/TiO ₂	–	Oxidizes materials photo-catalytically by using visible light	Indoor and outdoor air purification	[162]
BiNPs/TiO ₂	Facile eco-friendly synthesis	response to visible light and shows plasmon mediated activation	remove NO from air	[163]
TiO ₂ /r-GO/Ag	Facile one-pot hydrothermal	–	Remove formaldehyde from air	[185]
CQDs/Dots-TiO ₂	–	Responsive to visible light	Remove volatile organic compounds from air (benzene, toluene and p-xylene)	[186]
Carbon doped TiO ₂	Electrospinning	Absorb UV light with particle size 25–75 nm	Used in the photocatalysis of the Polycyclic Aromatic Hydrocarbon (PAH) dye	[187]
rGO/InVO ₄	Electrospinning	Responsive to visible light with particle size 250–400 nm	Remove rhodamine B by photocatalysis	[188]
Fe ₃ O ₄ /TiO ₂ /Ag	Sol-gel hydrothermal method	Responsive to both UV and visible light with particle size 10 nm	Photocatalysis of Ampicillin	[189]
BiOCl/Bi ₄ Ti ₃ O ₁₂	Solvothormal and electrospinning	Responsive to visible light	Photocatalysis of p-nitrophenol and methyl orange	[190]
Polyaniline coated TiO ₂ /SiO ₂	Electrospinning and in situ polymerization	Responsive to visible light	Removal of methyl orange by photocatalytic degradation	[191]

and cost-effective fabrication methods must be developed to produce high-quality materials in large quantities. Additionally, safety and environmental concerns are associated with using nanomaterials in photocatalytic applications. These materials' potential toxicity and impact on the environment need to be carefully evaluated and addressed.

Lastly, there is a need for standardization and regulation in the production and use of hybrid SC photocatalysts.^[200] Standardization of synthesis methods and characterization techniques will enable reproducibility and ensure the quality of the materials. Regulation will ensure these materials are safe and do not pose any risks to human health or the environment. In conclusion, developing hybrid SC photocatalyst nanomaterials for energy and environmental applications is a rapidly evolving field that faces several scientific challenges. Addressing these challenges will require collaboration between scientists, engineers, and policymakers to enable the successful implementation of these materials in practical applications.

7.3. Reasons Behind the Poor Stability

One of the significant challenges in developing hybrid SC photocatalyst nanomaterials for energy and environmental applications is their poor stability under various operating conditions. The stability of these materials is crucial for their long-term performance, durability, and commercial viability. The instability of hybrid SC photocatalysts can result from several factors, such as oxidation, reduction, hydrolysis, and surface contamination.^[192b] These factors can lead to the degradation of the materials over time, resulting in decreased photocatalytic activity and poor performance.^[201]

One common problem with hybrid SC photocatalysts is their susceptibility to photo corrosion. Photo corrosion occurs when the photocatalytic reaction forms reactive species, such as free radicals, which can cause damage to the material's surface and structure.^[202] This can lead to a loss of active sites and decreased photocatalytic activity. In addition, photo corrosion can release toxic species into the environment, which is a severe safety and environmental concern. Another factor contributing to the poor stability of hybrid SC photocatalysts is their sensitivity to environmental factors such as temperature, humidity, and pH.^[203] Exposure to high temperatures, humidity, or acidic/basic conditions can change the material's structure, composition, and properties, impacting its photocatalytic activity and stability.

Researchers are exploring several strategies to address the stability issues associated with hybrid SC photocatalysts.^[204] One approach is to modify the surface of the materials with protective coatings such as metal oxides or polymers, which can enhance their stability and prevent photo corrosion. Another strategy is to engineer the material's structure and morphology to reduce the likelihood of photo corrosion and improve stability. In addition, researchers are investigating alternative synthesis methods that can produce hybrid SC photocatalysts with enhanced stability.^[205] For example, sol-gel synthesis, hydrothermal synthesis, and microwave-assisted synthesis have been shown to produce more stable and durable photocatalysts compared to traditional methods.

Finally, long-term stability testing under realistic conditions is essential for evaluating the stability of hybrid SC photocatalyst nanomaterials. Standardized testing procedures that simulate real-world operating conditions are necessary to assess the durability and performance of these materials. In conclusion, improving the stability of hybrid SC photocatalyst nanomaterials is critical for their successful implementation in energy and environmental applications. Addressing the stability challenges associated with these materials will require a multidisciplinary approach involving materials synthesis, characterization, testing, and collaboration between scientists, engineers, and policymakers.

8. Importance of Density Functional Theory Calculations

In the previous sections, we discussed DFT calculations many times, so we need to know detail about the DFT as we know that some modifications are done in pristine photocatalysts to enhance its activity. These modifications are done by doping elements, fabricating composite, or synthesizing some new nano-hybrids. DFT calculations are the most powerful tool to know about the intrinsic mechanism behind the increased photocatalytic activity of photocatalysts, and it is also a type of fundamental calculation. DFT calculations mainly provide information about the following:

- Energy of photocatalyst.
- Geometric structure of atoms/molecules presents in photocatalyst.
- The optical and electronic properties of the photocatalysts.^[206]

In addition, DFT is a low-cost process that gives information about the material from the level of atom/molecule to the unit cell. Further DFT calculations provide all valuable information about the materials, i.e., the effect of doping elements over the geometry of the photocatalyst and its electronic properties.^[207] Further DFT calculations also give information about the interaction between the various components present in composites' adsorption of molecules with its photocatalytic mechanism over the surface of the photocatalyst. DFT calculations provide all information about the pre-existing modified and newly fabricated photocatalysts.^[208]

9. Conclusion and Future Outlook

In conclusion, hybrid SC photocatalyst nanomaterials have shown great potential for energy and environmental applications due to their unique properties and capabilities. Combining two or more different semiconductor materials has enhanced photocatalytic activity, stability, and selectivity, making them promising candidates for various applications such as water splitting, CO₂ reduction, and pollutant degradation. This review offers a comprehensive study of the properties, design, photocatalytic behavior, characterization, and application of hybrid SC-based nanomaterials as photocatalysts. The main application focused on in this article is renewable energy sources like photovoltaic solar cells, hydrogen production by the photochemical water splitting,

photo-assisted direct alcohol fuel cell, and some environmental applications like air and water remediation by using hybrid SC-based photocatalyst. The DFT calculation is also briefly discussed with some heterojunction hybrid semiconductor-based photocatalysts. As discussed in the article, these hybrid materials show good activity and better efficiency than single or pure materials and open a new door for researchers as hybrid semiconductors are multifunctional surfaces. Despite their many advantages, these hybrid materials have some disadvantages also. First, we take noble metals in most cases, which are very costly. Further, the synthesis approaches for these materials are also expensive. Further efforts will be made to synthesize these hybrid semiconductor nanomaterials as photocatalysts with different interfaces with low-cost, more reliable, large surface area and superior photocatalytic activity. Furthermore, attention should be given to earth-abundant-based photocatalysts with higher activity, selectivity, and profound stability. It is expected that the continued research will unlock the highly efficient co-catalyst hybrid semiconductor photocatalyst and enhance their contribution to photocatalysis.

Additional enhancement of the photocatalytic activity is also inherently connected to combining the SC-metal elements within HSPNs. Plasmonic photocatalysis has been drawing significant attraction currently. The metallic segment of the HSPNs may effectively absorb visible light via localized exterior plasmon resonance and transform it within holes and electrons into the nearby semiconductor. Harvesting and using the photons absorbed in the metal is anticipated to advance the general efficiency owing to the preferable metallic light-absorption features.

Finally, there is a considerable possibility for SC-metal hybrid NPs as photocatalysts. The tremendous advancements in the colloidal synthesis of NPs and a deeper insight into the physicochemical precepts that control the photocatalytic techniques pave the path toward optimal integration in current and future applications. Hybrid SC photocatalyst nanomaterials have a promising future in energy and environmental applications. Developing more efficient and stable nanomaterials through advanced synthesis techniques and incorporating new materials and functional groups will open up new avenues for research and applications. Using these nanomaterials in commercial applications is also expected to increase in the coming years, leading to a more sustainable and cleaner future.

Acknowledgements

The authors acknowledge the support from the Department of Chemistry and Research & Development Cell of Maharishi Markandeshwar (Deemed to be University), Mullana, Ambala, Haryana, India.

Conflict of Interest

The authors declare no conflict of interest.

Keywords

environmental applications, fuel cells, hybrid semiconductors nanomaterials, photocatalysts, photovoltaic cells

Received: March 7, 2023

Revised: May 16, 2023

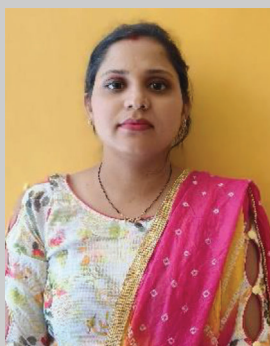
Published online:

- [1] a) K. Sheoran, H. Kaur, S. S. Siwal, V. K. Thakur, *Adv. Energy Sustainability Res.* **2023**, *n/a*, 2300021; b) S. S. Siwal, K. Sheoran, K. Mishra, H. Kaur, A. K. Saini, V. Saini, D.-V. N. Vo, H. Y. Nezhad, V. K. Thakur, *Chemosphere* **2022**, *293*, 133542; c) H. Kaur, V. K. Thakur, S. S. Siwal, *Mater Today Proc* **2022**, *56*, 112.
- [2] a) U. Banin, Y. Ben-Shahar, K. Vinokurov, *Chem. Mater.* **2014**, *26*, 97; b) A. Vaneski, A. S. Susha, J. Rodríguez-Fernández, M. Berr, F. Jäckel, J. Feldmann, A. L. Rogach, *Adv. Funct. Mater.* **2011**, *21*, 1547; c) K. Wu, T. Lian, *Chem. Soc. Rev.* **2016**, *45*, 3781.
- [3] Y. Ben-Shahar, U. Banin, in (Ed: A. Credi), Springer International Publishing, Cham **2017**.
- [4] R. Costi, A. E. Saunders, E. Elmalem, A. Salant, U. Banin, *Nano Lett.* **2008**, *8*, 637.
- [5] a) K. Wu, H. Zhu, T. Lian, *Acc. Chem. Res.* **2015**, *48*, 851; b) C. Gadiyar, A. Loiudice, R. Buonsanti, *J. Phys. D: Appl. Phys.* **2017**, *50*, 074006; c) K. Mishra, N. Devi, S. S. Siwal, Q. Zhang, W. F. Alsanie, F. Scarpa, V. K. Thakur, *Adv. Sci.* **2022**, *9*, 2202187; d) H. Lei, S. Singh Siwal, X. Zhang, Q. Zhang, *J. Colloid Interface Sci.* **2020**, *571*, 1; e) S. S. Siwal, W. Yang, Q. Zhang, *J. Energy Chem.* **2020**, *51*, 113; f) W. Yang, Q. Zhang, S. S. Siwal, Y. Hua, C. Xu, *Electrochim. Acta* **2020**, *137038*.
- [6] a) O. K. Varghese, M. Paulose, T. J. LaTempa, C. A. Grimes, *Nano Lett.* **2009**, *9*, 731; b) S. C. Roy, O. K. Varghese, M. Paulose, C. A. Grimes, *ACS Nano* **2010**, *4*, 1259; c) A. Manzi, T. Simon, C. Sonnleitner, M. Döblinger, R. Wyrwich, O. Stern, J. K. Stolarczyk, J. Feldmann, *J. Am. Chem. Soc.* **2015**, *137*, 14007.
- [7] N. Waikopf, Y. Ben-Shahar, U. Banin, *Adv. Mater.* **2018**, *30*, 1706697.
- [8] a) F. W. Krainer, A. Glieder, *Appl. Microbiol. Biotechnol.* **2015**, *99*, 1611; b) J.-X. Fan, M.-D. Liu, C.-X. Li, S. Hong, D.-W. Zheng, X.-H. Liu, S. Chen, H. Cheng, X.-Z. Zhang, *Nanoscale Horiz.* **2017**, *2*, 349.
- [9] a) W. He, H.-K. Kim, W. G. Wamer, D. Melka, J. H. Callahan, J.-J. Yin, *J. Am. Chem. Soc.* **2014**, *136*, 750; b) S. S. Siwal, Q. Zhang, A. K. Saini, V. K. Thakur, *J. Renewable Mater.* **2020**, *8*, 1543.
- [10] A. A. Pawar, S. Halivni, N. Waikopf, Y. Ben-Shahar, M. Soreni-Harari, S. Bergbreiter, U. Banin, S. Magdassi, *Nano Lett.* **2017**, *17*, 4497.
- [11] S. Zhong, Y. Xi, S. Wu, Q. Liu, L. Zhao, S. Bai, *J. Mater. Chem. A* **2020**, *8*, 14863.
- [12] L. J. Fang, X. L. Wang, Y. H. Li, P. F. Liu, Y. L. Wang, H. D. Zeng, H. G. Yang, *Appl. Catal., B* **2017**, *200*, 578.
- [13] S. Siwal, N. Devi, V. Perla, R. Barik, S. Ghosh, K. Mallick, *Mater. Res. Innovations* **2018**, *440*.
- [14] C. Prasad, Q. Liu, H. Tang, G. Yuvaraja, J. Long, A. Rammohan, G. V. Zyryanov, *J. Mol. Liq.* **2020**, *297*, 111826.
- [15] J. Peng, X. Chen, W.-J. Ong, X. Zhao, N. Li, *Chem* **2019**, *5*, 18.
- [16] R. Shen, L. Hao, Y. H. Ng, P. Zhang, A. Arramel, Y. Li, X. Li, *Chin. J. Catal.* **2022**, *43*, 2453.
- [17] X. Yan, B. Wang, M. Ji, Q. Jiang, G. Liu, P. Liu, S. Yin, H. Li, J. J. Xia, *Chin. J. Struct. Chem.* **2022**, *41*, 2208044.
- [18] N. B. Saber, A. Mezni, A. Alrooqi, T. Altalhi, *J. Mater Res Technol* **2020**, *9*, 15233.
- [19] H.-Y. Liu, C. C. Cody, J. A. Jayworth, R. H. Crabtree, G. W. Brudvig, *ACS Energy Lett.* **2020**, *5*, 3195.
- [20] a) T. Mokari, E. Rothenberg, I. Popov, R. Costi, U. Banin, *Science* **2004**, *304*, 1787; b) A. E. Saunders, I. Popov, U. Banin, *J. Phys. Chem. B* **2006**, *110*, 25421.
- [21] L. Tsybeskov, M. Alam, S. B. Hafiz, D. K. Ko, A. M. Bratkovsky, X. Wu, D. J. Lockwood, *J. Appl. Phys.* **2020**, *128*, 134301.

- [22] a) K. K. Haldar, T. Sen, S. Mandal, A. Patra, *ChemPhysChem* **2012**, *13*, 3989; b) H. Kaur, S. S. Siwal, R. V. Saini, N. Singh, V. K. Thakur, *ACS Nanosci Au* **2023**, *3*, 1.
- [23] J. Li, J. Z. Zhang, *Coord. Chem. Rev.* **2009**, *253*, 3015.
- [24] M. Li, X.-F. Yu, S. Liang, X.-N. Peng, Z.-J. Yang, Y.-L. Wang, Q.-Q. Wang, *Adv. Funct. Mater.* **2011**, *21*, 1788.
- [25] V. Lughi, in (Ed: B. Bhushan), Springer Netherlands, Dordrecht **2012**.
- [26] D. Steiner, T. Mokari, U. Banin, O. Millo, *Phys. Rev. Lett.* **2005**, *95*, 056805.
- [27] Y. Bekenstein, K. Vinokurov, U. Banin, O. Millo, *Nanotechnology* **2012**, *23*, 505710.
- [28] A. Wood, M. Giersig, P. Mulvaney, *J. Phys. Chem. B* **2001**, *105*, 8810.
- [29] D. Nandi, A. Taher, R. U. Islam, M. Choudhary, S. Siwal, K. Mallick, *Sci. Rep.* **2016**, *6*, 33025.
- [30] a) P. Yu, X. Wen, Y.-C. Lee, W.-C. Lee, C.-C. Kang, J. Tang, *J. Phys. Chem. Lett.* **2013**, *4*, 3596; b) T. Hirakawa, P. V. Kamat, *Langmuir* **2004**, *20*, 5645.
- [31] V. Subramanian, E. E. Wolf, P. V. Kamat, *J. Phys. Chem. B* **2003**, *107*, 7479.
- [32] D. Mongin, E. Shaviv, P. Maioli, A. Crut, U. Banin, N. Del Fatti, F. Vallée, *ACS Nano* **2012**, *6*, 7034.
- [33] F. V. A. Camargo, Y. Ben-Shahar, T. Nagahara, Y. E. Panfil, M. Russo, U. Banin, G. Cerullo, *Nano Lett.* **2021**, *21*, 1461.
- [34] a) K. Mishra, S. Singh Siwal, A. Kumar Saini, V. K. Thakur, *Fuel* **2023**, *332*, 126169; b) K. Sheoran, H. Kaur, S. S. Siwal, A. K. Saini, D.-V. N. Vo, V. K. Thakur, *Chemosphere* **2022**, *299*, 134364; c) S. S. Siwal, H. Kaur, R. Deng, Q. Zhang, *Curr Opin Green Sustain Chem* **2023**, *39*, 100722.
- [35] S. S. Siwal, H. Kaur, A. K. Saini, V. K. Thakur, *Adv. Energy Sustainability Res.* **2022**, *3*, 2200062.
- [36] F. Opoku, K. K. Govender, C. G. C. E. van Sittert, P. P. Govender, *Adv. Sustainable Syst.* **2017**, *1*, 1700006.
- [37] S. Porcu, F. Secci, P. C. Ricci, *Molecules* **2022**, *27*, 6828.
- [38] K. Maeda, *Adv. Mater.* **2019**, *31*, 1808205.
- [39] K. Maeda, K. Sekizawa, O. Ishitani, *Chem. Commun.* **2013**, *49*, 10127.
- [40] K. Wada, C. S. K. Ranasinghe, R. Kuriki, A. Yamakata, O. Ishitani, K. Maeda, *ACS Appl. Mater. Interfaces* **2017**, *9*, 23869.
- [41] J. Aliaga, N. Cifuentes, G. González, C. Sotomayor-Torres, E. Benavente, *Catalysts* **2018**, *8*, 374.
- [42] S. M. Kim, S. J. Lee, S. H. Kim, S. Kwon, K. J. Yee, H. Song, G. A. Somorjai, J. Y. Park, *Nano Lett.* **2013**, *13*, 1352.
- [43] N. Uddin, Z. Sun, J. Langley, H. Lu, P. Cao, A. Wibowo, X. Yin, C. S. Tang, H. T. Nguyen, J. D. Evans, X. Li, X. Zhang, M. Heggen, R. E. Dunin-Borkowski, A. T. S. Wee, H. Zhao, N. Cox, Z. Yin, *Proc. Natl. Acad. Sci. USA* **2023**, *120*, e2212075120.
- [44] C. Lin, H. Liu, M. Guo, Y. Zhao, X. Su, P. Zhang, Y. Zhang, *Colloids Surf. A* **2022**, *646*, 128962.
- [45] J. Li, Z. Lou, B. Li, *Chin. Chem. Lett.* **2022**, *33*, 1154.
- [46] Z. Liang, R. Shen, Y. H. Ng, Y. Fu, T. Ma, P. Zhang, Y. Li, X. Li, *Chem Catalysis* **2022**, *2*, 2157.
- [47] X. Li, J. Liu, J. Huang, C. He, Z. Feng, Z. Chen, L. Wan, F. Deng, *Wuli Huaxue Xuebao* **2020**, *37*, 2010030.
- [48] S. Bai, J. Jiang, Q. Zhang, Y. Xiong, *Chem. Soc. Rev.* **2015**, *44*, 2893.
- [49] a) Y. Bi, S. Ouyang, N. Umezawa, J. Cao, J. Ye, *J. Am. Chem. Soc.* **2011**, *133*, 6490; b) L. Liu, H. Zhao, J. M. Andino, Y. Li, *ACS Catal.* **2012**, *2*, 1817.
- [50] a) A. S. Cherevan, P. Gebhardt, C. J. Shearer, M. Matsukawa, K. Domen, D. Eder, *Energy Environ. Sci.* **2014**, *7*, 791; b) S. Bai, J. Ge, L. Wang, M. Gong, M. Deng, Q. Kong, L. Song, J. Jiang, Q. Zhang, Y. Luo, Y. Xie, Y. Xiong, *Adv. Mater.* **2014**, *26*, 5689.
- [51] S. Bai, W. Jiang, Z. Li, Y. Xiong, *ChemNanoMat* **2015**, *1*, 223.
- [52] a) B. Sun, Z. Liang, Y. Qian, X. Xu, Y. Han, J. Tian, *ACS Appl. Mater. Interfaces* **2020**, *12*, 7257; b) S. Ghosh, S. Bera, in *2D Materials for Energy Storage and Conversion*, IOP Publishing, **2021**; pp 8.1–8.59.
- [53] N. Uddin, H. Zhang, Y. Du, G. Jia, S. Wang, Z. Yin, *Adv. Mater.* **2020**, *32*, 1905739.
- [54] K.-W. Park, J.-H. Choi, B.-K. Kwon, S.-A. Lee, Y.-E. Sung, H.-Y. Ha, S.-A. Hong, H. Kim, A. Wieckowski, *J. Phys. Chem. B* **2002**, *106*, 1869.
- [55] S. Che, L. Zhang, T. Wang, D. Su, C. Wang, *Adv. Sustainable Syst.* **2022**, *6*, 2100294.
- [56] a) J. Zhang, Q. Xu, S. Z. Qiao, J. Yu, *ChemSusChem* **2013**, *6*, 2009; b) E. S. Agorku, M. A. Mamo, B. B. Mamba, A. C. Pandey, A. K. Mishra, *J. Porous Mater.* **2015**, *22*, 47.
- [57] P. Kanhere, Y. Tang, J. Zheng, Z. Chen, *J. Phys. Chem. Solids* **2013**, *74*, 1708.
- [58] L. M. Torres-Martínez, R. Gómez, O. Vázquez-Cuchillo, I. Juárez-Ramírez, A. Cruz-López, F. J. Alejandro-Sandoval, *Catal. Commun.* **2010**, *12*, 268.
- [59] a) L. Liu, P. Li, B. Adisak, S. Ouyang, N. Umezawa, J. Ye, R. Kodyath, T. Tanabe, G. V. Ramesh, S. Ueda, H. Abe, *J. Mater. Chem. A* **2014**, *2*, 9875; b) S. Kawasaki, R. Takahashi, K. Akagi, J. Yoshinobu, F. Komori, K. Horiba, H. Kumigashira, K. Iwashina, A. Kudo, M. Lippmaa, *J. Phys. Chem. C* **2014**, *118*, 20222.
- [60] a) J.-G. Ma, C.-R. Zhang, J.-J. Gong, Y.-Z. Wu, S.-Z. Kou, H. Yang, Y.-H. Chen, Z.-J. Liu, H.-S. Chen, *Materials* **2015**, *8*, 5508; b) B. K. Avsarala, S. R. Tirukkovalluri, S. Bojja, *Int. J. Mater. Res.* **2010**, *101*, 1563.
- [61] a) L. She, G. Tan, H. Ren, J. Huang, C. Xu, A. Xia, *RSC Adv.* **2015**, *5*, 36642; b) J. Tao, M. Yang, J. W. Chai, J. S. Pan, Y. P. Feng, S. J. Wang, *J. Phys. Chem. C* **2014**, *118*, 994.
- [62] a) Y. Xie, C. Yuan, *Appl. Catal., B* **2003**, *46*, 251; b) E. S. Agorku, H. Mittal, B. B. Mamba, A. C. Pandey, A. K. Mishra, *Int. J. Biol. Macromol.* **2014**, *70*, 143.
- [63] J. Li, T. Zhao, T. Chen, Y. Liu, C. N. Ong, J. Xie, *Nanoscale* **2015**, *7*, 7502.
- [64] J. Schneidewind, M. A. Argüello Cordero, H. Junge, S. Lochbrunner, M. Beller, *Energy Environ. Sci.* **2021**, *14*, 4427.
- [65] Q. Wang, T. Hisatomi, S. S. K. Ma, Y. Li, K. Domen, *Chem. Mater.* **2014**, *26*, 4144.
- [66] a) Y. Bai, C. Li, L. Liu, Y. Yamaguchi, M. Bahri, H. Yang, A. Gardner, M. A. Zwijnenburg, N. D. Browning, A. J. Cowan, A. Kudo, A. I. Cooper, R. S. Sprick, *Angew. Chem., Int. Ed.* **2022**, *61*, e202201299; b) B. Wu, R. Kempt, E. Kovalska, J. Luxa, A. Kuc, T. Heine, Z. Sofer, *ACS Appl. Nano Mater.* **2021**, *4*, 441.
- [67] a) X. Gao, Y. Shen, J. Liu, L. Lv, M. Zhou, Z. Zhou, Y. P. Feng, L. Shen, *J. Mater. Chem. C* **2021**, *9*, 15026; b) Y. Liu, R. Li, H. Yang, J. Song, J. Hu, C. Yang, Z. Zheng, *Int. J. Hydrogen Energy* **2022**, *47*, 14563.
- [68] a) F. Wang, Y. Jiang, A. Gautam, Y. Li, R. Amal, *ACS Catal.* **2014**, *4*, 1451; b) L. Hu, Y. Li, X. Peng, W. Zheng, W. Xu, J. Zhu, L. Y. S. Lee, P. K. Chu, K.-Y. Wong, *Chem. Eng. J.* **2021**, *417*, 127900.
- [69] a) C. Zhao, A. Krall, H. Zhao, Q. Zhang, Y. Li, *Int. J. Hydrogen Energy* **2012**, *37*, 9967; b) K. Huang, C. Li, Y. Zheng, L. Wang, W. Wang, X. Meng, *Sep. Purif. Technol.* **2022**, *283*, 120194.
- [70] P. D. Tran, L. Xi, S. K. Batabyal, L. H. Wong, J. Barber, J. S. Chye Loo, *Phys. Chem. Chem. Phys.* **2012**, *14*, 11596.
- [71] W. Wang, S. Liu, L. Nie, B. Cheng, J. Yu, *Phys. Chem. Chem. Phys.* **2013**, *15*, 12033.
- [72] W. J. Foo, C. Zhang, G. W. Ho, *Nanoscale* **2013**, *5*, 759.
- [73] A.-W. Xu, Y. Gao, H.-Q. Liu, *J. Catal.* **2002**, *207*, 151.
- [74] J. Madhavi, V. Prasad, K. R. Reddy, C. Venkata Reddy, A. V. Raghu, *J. Environ. Chem. Eng.* **2021**, *9*, 106335.
- [75] M. Guo, J. Du, *Phys. B* **2012**, *407*, 1003.
- [76] X. Li, S. Wu, P. Hu, X. Xing, Y. Liu, Y. Yu, M. Yang, J. Lu, S. Li, W. Liu, *J. Appl. Phys.* **2009**, *106*, 043913.
- [77] M. L. Guo, X. D. Zhang, C. T. Liang, *Phys. B* **2011**, *406*, 3354.

- [78] a) P. S. Basavarajappa, S. B. Patil, N. Ganganagappa, K. R. Reddy, A. V. Raghu, C. V. Reddy, *Int. J. Hydrogen Energy* **2020**, *45*, 7764; b) S. S. Siwal, Q. Zhang, A. K. Saini, V. K. Gupta, D. Roberts, V. Saini, F. Coulon, B. Pareek, V. K. Thakur, *J. Environ. Chem. Eng.* **2021**, *9*, 105982.
- [79] J. T. Park, D. J. Kim, D. H. Kim, J. H. Kim, *Mater. Lett.* **2017**, *202*, 66.
- [80] T. Boningari, S. N. R. Inturi, M. Suidan, P. G. Smirniotis, *Chem. Eng. J.* **2018**, *339*, 249.
- [81] J. Shao, W. Sheng, M. Wang, S. Li, J. Chen, Y. Zhang, S. Cao, *Appl. Catal., B* **2017**, *209*, 311.
- [82] a) M. N. Uddin, M. S. Islam, M. M. R. Mazumder, M. A. Hossain, M. Elias, I. A. Siddiquey, M. A. B. H. Susan, D. K. Saha, M. M. Rahman, A. M. Asiri, S. Hayami, J. *Inclusion Phenom. Macrocyclic Chem.* **2015**, *82*, 229; b) W. Anku, S. O.-B. Oppong, S. K. Shukla, P. P. J. A. C. S. Govender, *Acta Chim. Slov.* **2016**, *63*, 380.
- [83] Y. Jiang, H. Yuan, H. Chen, *Phys. Chem. Chem. Phys.* **2015**, *17*, 630.
- [84] Y. Wu, M. Xing, J. Zhang, F. Chen, *Appl. Catal., B* **2010**, *97*, 182.
- [85] F. Armano, K. Nogami, B. Ohtani, *Catal. Commun.* **2012**, *20*, 12.
- [86] H. Yan, X. Wang, M. Yao, X. Yao, *Prog. Nat. Sci.: Mater. Int.* **2013**, *23*, 402.
- [87] F. Wang, Z. Ma, P. Ban, X. Xu, *Mater. Lett.* **2017**, *195*, 143.
- [88] B. Modak, K. Srinivasu, S. K. Ghosh, *J. Phys. Chem. C* **2014**, *118*, 10711.
- [89] H. Li, L. Chen, S. Liu, C. Li, J. Meng, Z. J. M. S.-P. Wang, *Mater. Sci.-Poland* **2015**, *33*, 549.
- [90] B. Modak, K. Srinivasu, S. K. Ghosh, *RSC Adv.* **2014**, *4*, 45703.
- [91] M. Liras, M. Barawi, V. A. de la Peña O'Shea, *Chem. Soc. Rev.* **2019**, *48*, 5454.
- [92] R. Yang, Y. Zhang, Y. Fan, R. Wang, R. Zhu, Y. Tang, Z. Yin, Z. Zeng, *Chem. Eng. J.* **2022**, *428*, 131145.
- [93] K. Mishra, N. Devi, S. S. Siwal, V. K. Thakur, *Appl. Catal., B* **2023**, *334*, 122820.
- [94] Z. Wang, Z. Sun, H. Yin, X. Liu, J. Wang, H. Zhao, C. H. Pang, T. Wu, S. Li, Z. Yin, X.-F. Yu, *Adv. Mater.* **2022**, *34*, 2104113.
- [95] H. Lu, J. Tournet, K. Dastafkan, Y. Liu, Y. H. Ng, S. K. Karuturi, C. Zhao, Z. Yin, *Chem. Rev.* **2021**, *121*, 10271.
- [96] in (Ed: M. A. Green), Springer Berlin Heidelberg, Berlin, Heidelberg **2003**.
- [97] a) M. S. Tomar, F. J. Garcia, *Thin Solid Films* **1982**, *90*, 419; b) K. D. Dobson, I. Visoly-Fisher, G. Hodes, D. Cahen, *Sol. Energy Mater. Sol. Cells* **2000**, *62*, 295.
- [98] S. Iijima, *Nature* **1991**, *354*, 56.
- [99] C. Li, F. Wang, J. C. Yu, *Energy Environ. Sci.* **2011**, *4*, 100.
- [100] R. R. Lunt, V. Bulovic, *Appl. Phys. Lett.* **2011**, *98*, 113305.
- [101] G. Zhang, S. Finefrock, D. Liang, G. G. Yadav, H. Yang, H. Fang, Y. Wu, *Nanoscale* **2011**, *3*, 2430.
- [102] J. M. Luther, M. Law, M. C. Beard, Q. Song, M. O. Reese, R. J. Ellingson, A. J. Nozik, *Nano Lett.* **2008**, *8*, 3488.
- [103] J.-C. Lee, W. Lee, S.-H. Han, T. G. Kim, Y.-M. Sung, *Electrochem. Commun.* **2009**, *11*, 231.
- [104] I. Bouziani, M. Kibbou, Z. Haman, N. Khossossi, I. Essaoudi, A. Ainane, R. Ahuja, *Phys. E* **2021**, *134*, 114900.
- [105] a) S. Licht, *J. Phys. Chem. B* **2003**, *107*, 4253; b) B. O'Regan, M. Grätzel, *Nature* **1991**, *353*, 737.
- [106] M. Z. Iqbal, S. Siddique, *Int. J. Hydrogen Energy* **2018**, *43*, 21502.
- [107] R. Dillert, D. H. Taffa, M. Wark, T. Bredow, D. W. Bahnemann, *APL Mater.* **2015**, *3*, 104001.
- [108] L. Pan, S. Wang, J. Xie, L. Wang, X. Zhang, J.-J. Zou, *Nano Energy* **2016**, *28*, 296.
- [109] X. Gan, D. Lei, *Coord. Chem. Rev.* **2022**, *469*, 214665.
- [110] M. Tayebi, B.-K. Lee, *Renewable Sustainable Energy Rev.* **2019**, *111*, 332.
- [111] S. K. Saraswat, D. D. Rodene, R. B. Gupta, *Renewable Sustainable Energy Rev.* **2018**, *89*, 228.
- [112] T. Ishaq, M. Yousaf, I. A. Bhatti, A. Batool, M. A. Asghar, M. Mohsin, M. Ahmad, *Int. J. Hydrogen Energy* **2021**, *46*, 39036.
- [113] J. Jiang, Z. Xiong, H. Wang, G. Liao, S. Bai, J. Zou, P. Wu, P. Zhang, X. Li, *J. Mater. Sci. Technol.* **2022**, *118*, 15.
- [114] J. Huang, C. Li, X. Hu, J. Fan, B. Zhao, E. J. Liu, *Chin. J. Struct. Chem.* **2022**, *41*, 62.
- [115] Z. Zhao, K. Dai, J. Zhang, G. Dawson, *Adv. Sustainable Syst.* **2023**, *7*, 2100498.
- [116] W. Chen, X. Li, F. Wang, S. Javadi, Y. Pang, J. Chen, Z. Yin, S. Wang, Y. Li, G. Jia, *Small* **2020**, *16*, 1902231.
- [117] W. Zhou, Z. Yin, Y. Du, X. Huang, Z. Zeng, Z. Fan, H. Liu, J. Wang, H. Zhang, *Small* **2013**, *9*, 140.
- [118] H. Wang, L. Chen, Y. Sun, J. Yu, Y. Zhao, X. Zhan, H. Shi, *Sep. Purif. Technol.* **2021**, *265*, 118516.
- [119] J. Bai, R. Shen, Z. Jiang, P. Zhang, Y. Li, X. Li, *Chin. J. Catal.* **2022**, *43*, 359.
- [120] Z. Fan, X. Guo, Z. Jin, X. Li, Y. Li, *Langmuir* **2022**, *38*, 3244.
- [121] Z. Lei, X. Ma, X. Hu, J. Fan, E. J. Liu, *Acta. Phys. Chim. Sin.* **2022**, *38*, 2110049.
- [122] J. Bai, W. Chen, R. Shen, Z. Jiang, P. Zhang, W. Liu, X. Li, *J. Mater. Sci. Technol.* **2022**, *112*, 85.
- [123] R. Shen, L. Zhang, N. Li, Z. Lou, T. Ma, P. Zhang, Y. Li, X. Li, *ACS Catal.* **2022**, *12*, 9994.
- [124] R. Shen, Y. Ding, S. Li, P. Zhang, Q. Xiang, Y. H. Ng, X. Li, *Chin. J. Catal.* **2021**, *42*, 25.
- [125] J. Fang, L. Xu, Z. Zhang, Y. Yuan, S. Cao, Z. Wang, L. Yin, Y. Liao, C. Xue, *ACS Appl. Mater. Interfaces* **2013**, *5*, 8088.
- [126] Z. Liang, R. Shen, P. Zhang, Y. Li, N. Li, X. Li, *Chin. J. Catal.* **2022**, *43*, 2581.
- [127] K. Mishra, V. Kumar Thakur, S. Singh Siwal, *Mater Today Proc* **2022**, *56*, 107.
- [128] F. Bensebaa, A. A. Farah, D. Wang, C. Bock, X. Du, J. Kung, Y. L. Page, *J. Phys. Chem. B* **2005**, *109*, 15339.
- [129] A. Kaur, G. Kaur, P. P. Singh, S. Kaushal, *Int. J. Hydrogen Energy* **2021**, *46*, 15820.
- [130] S. Siwal, S. Matseke, S. Mpelane, N. Hooda, D. Nandi, K. Mallick, *Int. J. Hydrogen Energy* **2017**, *42*, 23599.
- [131] S. Siwal, N. Devi, V. K. Perla, S. K. Ghosh, K. Mallick, *Catal., Struct. React.* **2019**, *5*, 1.
- [132] a) L. Xiong, A. Manthiram, *Electrochim. Acta* **2004**, *49*, 4163; b) J. Shim, C.-R. Lee, H.-K. Lee, J.-S. Lee, E. J. Cairns, *J. Power Sources* **2001**, *102*, 172.
- [133] K. Drew, G. Girishkumar, K. Vinodgopal, P. V. Kamat, *J. Phys. Chem. B* **2005**, *109*, 11851.
- [134] C.-T. Lin, H. J. Huang, J.-J. Yang, M.-H. Shiao, *Microelectron. Eng.* **2011**, *88*, 2644.
- [135] J. Hu, C. Zhai, M. Zhu, *Chin. Chem. Lett.* **2021**, *32*, 1348.
- [136] B. Bateer, Y. Qu, C. Tian, S. Du, Z. Ren, R. Wang, K. Pan, H. Fu, *Mater. Res. Bull.* **2014**, *56*, 34.
- [137] C. Zhai, M. Zhu, F. Pang, D. Bin, C. Lu, M. C. Goh, P. Yang, Y. Du, *ACS Appl. Mater. Interfaces* **2016**, *8*, 5972.
- [138] C. Odetola, L. N. Trevani, E. B. Easton, *Appl. Catal., B* **2017**, *210*, 263.
- [139] X. Hu, C. Ge, N. Su, H. Huang, Y. Xu, J. Zhang, J. Shi, X. Shen, N. Saito, *J. Alloys Compd.* **2017**, *692*, 848.
- [140] D. Chu, S. Wang, P. Zheng, J. Wang, L. Zha, Y. Hou, J. He, Y. Xiao, H. Lin, Z. Tian, *ChemSusChem* **2009**, *2*, 171.
- [141] A. Leelavathi, G. Madras, N. Ravishankar, *J. Am. Chem. Soc.* **2014**, *136*, 14445.
- [142] A. Arabzadeh, A. Salimi, M. Ashrafi, S. Soltanian, P. Servati, *Catal. Sci. Technol.* **2016**, *6*, 3485.
- [143] M. G. Hosseini, M. M. Momeni, *Fuel Cells* **2012**, *12*, 406.
- [144] H. Gao, C. Zhai, C. Yuan, Z.-Q. Liu, M. Zhu, *Electrochim. Acta* **2020**, *330*, 135214.
- [145] C. Zhai, J. Hu, M. Sun, M. Zhu, *Appl. Surf. Sci.* **2018**, *430*, 578.

- [146] J. Zhang, X. Hu, F. Zhu, N. Su, H. Huang, J. Cheng, H. Yang, *Nanotechnology* **2017**, *28*, 505603.
- [147] M. Zhu, C. Zhai, M. Sun, Y. Hu, B. Yan, Y. Du, *Appl. Catal., B* **2017**, *203*, 108.
- [148] R. He, R. Chen, J. Luo, S. Zhang, D. Xu, *Wuli Huaxue Xuebao* **2020**, *37*, 2011022.
- [149] T. Yang, P. Deng, L. Wang, J. Hu, Q. Liu, H. J. Tang, *Chin. J. Struct. Chem.* **2022**, *41*, 23.
- [150] K. Mondal, *Inventions* **2017**, *2*, 9.
- [151] a) S. Li, M. Cai, C. Wang, Y. Liu, N. Li, P. Zhang, X. Li, *J. Mater. Sci. Technol.* **2022**, *123*, 177; b) K. Mishra, S. S. Siwal, S. C. Nayaka, Z. Guan, V. K. Thakur, *Sci. Total Environ.* **2023**, *887*, 164006.
- [152] K. A. Abd-El Salam, in (Ed: K. A. Abd-El Salam), Elsevier, **2020**.
- [153] S. S. Siwal, Q. Zhang, N. Devi, K. V. Thakur, *Polymers* **2020**, *12*, 505.
- [154] N. Li, J. Ma, Y. Zhang, L. Zhang, T. Jiao, *Adv. Sustainable Syst.* **2022**, *6*, 2200106.
- [155] L. Yang, D. Fan, Z. Li, Y. Cheng, X. Yang, T. Zhang, *Adv. Sustainable Syst.* **2022**, *6*, 2100477.
- [156] S. Mukhopadhyay, D. Maiti, S. Chatterjee, P. S. Devi, G. S. Kumar, *Phys. Chem. Chem. Phys.* **2016**, *18*, 31622.
- [157] J. Gröttrup, F. Schütt, D. Smazna, O. Lupan, R. Adelung, Y. K. Mishra, *Ceram. Int.* **2017**, *43*, 14915.
- [158] H. Liu, J. P. Nkundabose, H. Chen, L. Yang, C. Meng, N. Ding, *J. Environ. Chem. Eng.* **2022**, *10*, 107154.
- [159] S. Li, M. Cai, Y. Liu, J. Zhang, C. Wang, S. Zang, Y. Li, P. Zhang, X. Li, *Inorg. Chem. Front.* **2022**, *9*, 2479.
- [160] D. Zhou, L. Wang, F. Zhang, J. Wu, H. Wang, J. Yang, *Adv. Sustainable Syst.* **2022**, *6*, 2100516.
- [161] a) R. M. Alberici, W. F. Jardim, *Appl. Catal., B* **1997**, *14*, 55; b) H. Yu, K. Zhang, C. Rossi, *Indoor Built Environ* **2007**, *16*, 529.
- [162] F. Petronella, A. Truppi, M. Striccoli, M. L. Curri, R. Comparelli, in (Eds: S. Mohapatra, T. A. Nguyen, P. Nguyen-Tri), Woodhead Publishing, **2019**.
- [163] Z. Zhao, W. Zhang, X. Lv, Y. Sun, F. Dong, Y. Zhang, *Environ. Sci.: Nano* **2016**, *3*, 1306.
- [164] A. Ahmad, M. Ali, A. G. Al-Sehemi, A. A. Al-Ghamdi, J.-W. Park, H. Algarni, H. Anwer, *Chem. Eng. J.* **2023**, *452*, 139436.
- [165] Y. Zhang, S. He, W. Guo, Y. Hu, J. Huang, J. R. Mulcahy, W. D. Wei, *Chem. Rev.* **2018**, *118*, 2927.
- [166] P. Madhusudan, R. Shi, S. Xiang, M. Jin, B. N. Chandrashekar, J. Wang, W. Wang, O. Peng, A. Amini, C. Cheng, *Appl. Catal., B* **2021**, *282*, 119600.
- [167] P. Chen, Z. Guo, X. Liu, H. Lv, Y. Che, R. Bai, Y. Chi, H. Xing, *J. Mater. Chem. A* **2019**, *7*, 27074.
- [168] a) S. S. Sreejith, N. Mohan, M. R. P. Kurup, in (Eds.: L. R. Thoutam, S. Tayal, J. Ajayan), Springer Nature Singapore, Singapore **2022**; b) M. Bashir, S. Aman, A. Awan, M. F. Nazar, M. Zubair, R. Nadeem, M. N. Zafar, in (Eds: A. E. Shalan, A. S. Hamdy Makhoulouf, S. Lanceros-Méndez), Springer International Publishing, Cham **2022**; c) H. Kaur, N. Devi, S. S. Siwal, W. F. Alsanie, M. K. Thakur, V. K. Thakur, *ACS Omega* **2023**, *8*, 9004.
- [169] S. Cheng, Z. Sun, K. H. Lim, T. Z. H. Gani, T. Zhang, Y. Wang, H. Yin, K. Liu, H. Guo, T. Du, L. Liu, G. K. Li, Z. Yin, S. Kawi, *Adv. Energy Mater.* **2022**, *12*, 2200389.
- [170] X. Yang, H. Fu, W. Wang, S. Xiong, D. Han, Z. Deng, X. An, *Appl. Surf. Sci.* **2020**, *505*, 144631.
- [171] T.-T. Zhuang, Y. Liu, M. Sun, S.-L. Jiang, M.-W. Zhang, X.-C. Wang, Q. Zhang, J. Jiang, S.-H. Yu, *Angew. Chem., Int. Ed.* **2015**, *54*, 11495.
- [172] H. Park, W. Choi, M. R. Hoffmann, *J. Mater. Chem.* **2008**, *18*, 2379.
- [173] M. An, L. Li, J. Zhang, L. Zhao, C. Yang, *J. Nanopart Res* **2019**, *21*, 117.
- [174] K. Flomin, M. Diab, T. Mokari, *Nanoscale* **2017**, *9*, 16138.
- [175] U. Caudillo-Flores, A. Kubacka, T. Berestok, T. Zhang, J. Llorca, J. Arbiol, A. Cabot, M. Fernández-García, *Int. J. Hydrogen Energy* **2020**, *45*, 1510.
- [176] Y. Zhang, J. Nie, Q. Wang, X. Zhang, Q. Wang, Y. Cong, *Appl. Surf. Sci.* **2018**, *427*, 1009.
- [177] S.-E. Kim, J.-Y. Woo, S.-Y. Kang, B. K. Min, J. K. Lee, S.-W. Lee, *J. Ind. Eng. Chem* **2016**, *43*, 142.
- [178] X. Cai, Q. Chen, R. Wang, A. Wang, J. Wang, S. Zhong, Y. Liu, J. Chen, S. Bai, *Adv. Mater. Interfaces* **2019**, *6*, 1900775.
- [179] X. Zhang, L. Wang, C. Liu, Y. Ding, S. Zhang, Y. Zeng, Y. Liu, S. Luo, *J. Hazard. Mater.* **2016**, *313*, 244.
- [180] Y. Jiao, H. Jiang, F. Chen, *ACS Catal.* **2014**, *4*, 2249.
- [181] R. A. Badhe, A. Ansari, S. S. Garje, *ACS Omega* **2018**, *3*, 18663.
- [182] J. Tao, Z. Gong, G. Yao, Y. Cheng, M. Zhang, J. Lv, S. Shi, G. He, X. Jiang, X. Chen, Z. Sun, *J. Alloys Compd.* **2016**, *688*, 605.
- [183] A. Azimi-Fouladi, S. A. Hassanzadeh-Tabrizi, A. Saffar-Teluri, *Ceram. Int.* **2018**, *44*, 4292.
- [184] K. Xu, J. Wu, C. F. Tan, G. W. Ho, A. Wei, M. Hong, *Nanoscale* **2017**, *9*, 11574.
- [185] Z. Jie, X. Xiao, Y. Huan, H. Youkang, Z. Zhiyao, *Environ. Technol.* **2021**, *42*, 193.
- [186] A. Mahmood, G. Shi, Z. Wang, Z. Rao, W. Xiao, X. Xie, J. Sun, *J. Hazard. Mater.* **2021**, *401*, 123402.
- [187] K. Mondal, S. Bhattacharyya, A. Sharma, *Ind. Eng. Chem. Res.* **2014**, *53*, 18900.
- [188] D. Ma, Y. Zhang, M. Gao, Y. Xin, J. Wu, N. Bao, *Appl. Surf. Sci.* **2015**, *353*, 118.
- [189] Y. Zhao, C. Tao, G. Xiao, G. Wei, L. Li, C. Liu, H. Su, *Nanoscale* **2016**, *8*, 5313.
- [190] M. Zhang, Y. Liu, L. Li, H. Gao, X. Zhang, *Catal. Commun.* **2015**, *58*, 122.
- [191] Z. Liu, Y.-E. Miao, M. Liu, Q. Ding, W. W. Tjui, X. Cui, T. Liu, *J. Colloid Interface Sci.* **2014**, *424*, 49.
- [192] a) P. D. Tran, L. H. Wong, J. Barber, J. S. C. Loo, *Energy Environ. Sci.* **2012**, *5*, 5902; b) W. Tu, Y. Zhou, Z. Zou, *Adv. Funct. Mater.* **2013**, *23*, 4996.
- [193] M. S. A. Che Mansor, M. N. I. Amir, N. Muhd Julkapli, A. Ma'amor, *Mater. Chem. Phys.* **2020**, *241*, 122415.
- [194] a) S. Banerjee, D. D. Dionysiou, S. C. Pillai, *Appl. Catal., B* **2015**, *176*, 396; b) K. Sheoran, S. S. Siwal, D. Kapoor, N. Singh, A. K. Saini, W. F. Alsanie, V. K. Thakur, *ACS Eng. Au* **2022**, *2*, 378.
- [195] A. B. A. Kayani, S. Kuriakose, M. Monshipouri, F. A. Khalid, S. Walia, S. Sriram, M. Bhaskaran, *Small* **2021**, *17*, 2100621.
- [196] S. Kumar, M. M. Malik, R. Purohit, *Mater Today Proc* **2017**, *4*, 350.
- [197] H. Cheng, J. Wang, Y. Zhao, X. Han, *RSC Adv.* **2014**, *4*, 47031.
- [198] V. K. Yemmireddy, Y.-C. Hung, *Compr Rev Food Sci Food Saf* **2017**, *16*, 617.
- [199] F. H. Abdullah, N. H. H. A. Bakar, M. A. Bakar, *J. Hazard. Mater.* **2022**, *424*, 127416.
- [200] H. Yang, K. Dai, J. Zhang, G. Dawson, *Chin. J. Catal.* **2022**, *43*, 2111.
- [201] H.-C. Liang, X.-Z. Li, *J. Hazard. Mater.* **2009**, *162*, 1415.
- [202] A. T. Le, N. S. B. Samsuddin, S.-L. Chiam, S.-Y. Pung, *Bull. Mater. Sci.* **2021**, *44*, 5.
- [203] H. Xu, L. Chen, D. J. McClements, Y. Hu, H. Cheng, C. Qiu, H. Ji, C. Sun, Y. Tian, M. Miao, Z. Jin, *Chem. Eng. J.* **2022**, *432*, 134301.
- [204] C. Han, X. Zhu, J. S. Martin, Y. Lin, S. Spears, Y. Yan, *ChemSusChem* **2020**, *13*, 4005.
- [205] H. Uk Lee, S. C. Lee, J. Won, B.-C. Son, S. Choi, Y. Kim, S. Y. Park, H.-S. Kim, Y.-C. Lee, J. Lee, *Sci. Rep.* **2015**, *5*, 8691.
- [206] Z. Bicheng, B. Cheng, L. Zhang, J. Yu, *Carbon Energy* **2019**, *1*, 32.
- [207] Y. zhang, Z. Wang, J. Cao, *J. Mater. Chem. C* **2014**, *2*, 8817.
- [208] Z. Bicheng, L. Zhang, D. Xu, B. Cheng, J. Yu, *J. CO2 Util.* **2017**, *21*, 327.



Kirti Mishra is currently carrying-out doctoral degree (under Dr. Samarjeet Singh Siwal and Prof. Vijay Kumar Thakur) at the Department of Chemistry, Maharishi Markandeshwar (Deemed to be University) Mullana, Ambala, India. She obtained her postgraduate degree in Chemistry and graduated from Kurukshetra University, Kurukshetra, India. Her research interests include material science, nanomaterials, polymer nanocomposites, electrochemistry, and ionic liquids.



Nishu Devi is a postdoctoral fellow at Northwestern University, Evanston, IL, USA and a Mechanics and Energy Lab member. Before joining MEL, she worked as a postdoctoral researcher at the University of Johannesburg and visiting researcher at CSIR-Pretoria, South Africa. Dr. Nishu obtained her doctorate in Chemistry from the University of Johannesburg, South Africa, on electrochemical energy storage devices and graduated with M.Tech. & B.Tech. in Chemical Engineering from DCR University of Science and Technology, India. Her research interests include material science, nanomaterials, polymer nanocomposites, electrochemistry, surface chemistry of electrodes, electrochemical energy storage, electrodeposition, and EMI shielding.



Samarjeet Singh Siwal is currently working as an associate professor in the Department of Chemistry, MM (DU), Mullana-India. He received his Ph.D. in Chemistry from the University of Johannesburg, South Africa, in 2017. Then, he moved to Kunming University of Science and Technology (KUST), China as a post-doctoral research fellow (under Prof. Qibo Zhang). His research interests include synthesizing and applying 2D materials in different fields, such as overall water splitting, supercapacitors, fuel cells, and biosensors. He has published over 80 SCI journal articles, 2 patents, and 06 book chapters.



Vijai Kumar Gupta is a senior fellow of the Biorefining and Advanced Materials Research Centre at SRUC, Edinburgh, UK. He is one of the leading experts in Biomass Valorization, Microbial Engineering Biotechnologies, Enzyme & Bioprocess Technology, Bioactive Natural Products, and Functional Microbiome Interactions. He has edited 42 books for internationally reputed publishers such as Elsevier, Wiley-Blackwell, Taylor and Francis, Springer-Nature, CABI, Nova Science, and De Gruyter. Also, he has published over 300 papers in internationally well-reputed journals with an author h-index of 74 and an i10 index of 331.



Vijay Kumar Thakur is a professor and head of the Biorefining and Advanced Materials Research Centre at SRUC, Edinburgh, UK. Before commencing his tenure at SRUC, he held faculty positions at Cranfield University, Washington State University, USA, and Nanyang Technological University, Singapore. His research activities span the disciplines of Biorefining, Chemistry, Manufacturing, Materials Science, Nanotechnology, and Sustainable and Advanced Materials. He has published over 360 SCI journal articles, 2 patents, 54 books, and 45 book chapters. He sits on the editorial board of several SCI journals as an Editor/Editorial Advisory Board member.